

Universidade Eduardo Mondlane

Solar PV-Based EV Charging Station for Urban Mobility: A Case Study of the proposed BRT Line N1 in the Maputo Metropolitan Area

Da-Costa, Manuel João

Dissertation submitted to the Eduardo Mondlane University as part of the requirements for the degree of Master of Science

Maputo, August 2026

Manuel João Da-Costa

Solar PV-Based EV Charging Station for Urban Mobility: A Case Study of the proposed BRT Line N1 in the Maputo Metropolitan Area

A Dissertation Submitted to the Faculty of Science of Eduardo Mondlane University as part of the Requirements for the Degree of Master of Science in Renewable Energy Science and Technology

Supervisor: Professor Doutor Boaventura Chongo Cuamba

Co-Supervisor: Prof. dr. Luis Consolo Chea

Maputo, August 2026

EDUARDO MONDLANE UNIVERSITY

FACULTY OF SCIENCES

POSTGRADUATE PROGRAM IN RENEWABLE ENERGY SCIENCE AND TECHNOLOGY (MCTER)

SOLAR PV-BASED EV CHARGING STATION FOR URBAN MOBILITY

A Case Study of the proposed BRT Line N1 in the Maputo Metropolitan Area

Manuel João Da-Costa

Dissertation presented to the Master's Program of the Department of Physics, Faculty of Science, Eduardo Mondlane University, as part of the requirements for the degree of Master of Science in Renewable Energy Science and Technology.

Approved in August 2026 by

Prof. Dr. Doroteia Hipoldina dos Santos Isaías
(Examiner- Department of Physics-UEM)

Prof. Dr. António Leão
(Chairperson of the examination committee- Department of Physics-UEM)

Prof. Dr. Boaventura Chongo Cuamba
(Supervisor- Department of Physics-UEM)

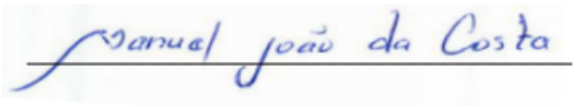
Prof. dr. Luis Consolo Chea
(Co-Supervisor- Department of Physics-UEM)

Maputo, 2026

Declaration and Authorship

I hereby declare that the dissertation entitled " Solar PV-Based EV Charging Station for Urban Mobility: A Case Study of the proposed BRT Line N1 in the Maputo Metropolitan Area " is my own original work and has not been submitted for any other degree or qualification. I further declare that all sources and references used in this dissertation have been properly cited in the text and are included in the list of references.

The candidate



13 August 2026

Acknowledgements

I would like to express my sincere gratitude to everyone who contributed, directly or indirectly, to the completion of this dissertation.

First and foremost, I thank God for the opportunities I have received and for guiding my path through yet another challenge.

I am deeply grateful to my supervisors, Professor Boaventura Chongo Cuamba and my co-supervisor, Professor dr Luis Consolo Chea, for their trust, availability, and invaluable guidance throughout this journey.

I would also like to thank my professors and colleagues for their encouragement, knowledge, and collaboration.

Finally, my heartfelt thanks go to my family for their unwavering support, understanding, and motivation at all times.

Abstract

Driven by the need to mitigate climate change, reduce urban air pollution, and decrease reliance on volatile fuel prices, this study explores the integration of Photovoltaic (PV) Systems into the charging infrastructure for electric buses (E-Buses), for the proposed Bus Rapid Transit (BRT) Line N1, in the Maputo Metropolitan Area (MMA). Considering the urban mobility pattern in Maputo, characterized by strong unidirectional flows and high peak-hour demand, the operational schedule was defined based on these critical periods. The E-bus load profile defined using a physical model, yielded an average specific energy consumption of 1.91 kWh/km at the powertrain level. The solar resource assessment, based on the Typical Meteorological Year (TMY) dataset sourced from PVGIS-SARA2 indicated an annual daily average global horizontal irradiation (GHI) of 5.2 kWh/m², and a global tilted irradiation (GTI) of 5.58 kWh/m² at the optimum tilt angle of 29º. Based on the daily load profile, and on the PVGIS dataset, two grid-connected, zero-export PV sizing scenarios were assessed, under strict self-consumption. Scenario-1, sized to meet full daily demand throughout the year, generated an average surplus of about 162. kWh/day, thereby justifying the integration of a Battery Energy Storage System (BESS). Scenario-2, optimised to match annual average demand, resulted in a near-zero net surplus, enabling high self-consumption and eliminating the need for a BESS, with occasional deficits supplied by the national grid. The findings demonstrate that PV-based E-bus charging is technically feasible and offers substantial environmental benefits, including up to 100% elimination of in-situ CO_2 emissions under full PV supply and complete removal of NOx and Particulate Matter (PM) emissions in all electrification scenarios. Overall, the study provides a replicable framework for integrating renewable energy and E-mobility as key enablers for the energy transition, both in Maputo and in other African cities.

Keywords: Energy Transition, Electric Vehicles, Urban mobility, Electric Buses, Solar resource

Resumo

Impulsionado pela necessidade de mitigar as alterações climáticas, reduzir a poluição atmosférica urbana e diminuir a dependência de preços voláteis dos combustíveis fósseis, este estudo explora a integração de sistemas fotovoltaicos (PV) na infraestrutura de carregamento de autocarros elétricos (E-Buses), no âmbito da proposta de implementação da linha N1 do sistema de Transporte Rápido por Autocarros (BRT), na Área Metropolitana de Maputo (AMM). Tendo em conta o padrão de mobilidade urbana em Maputo, caracterizado por fluxos unidireccionais intensos e picos de demanda em horas de ponta, o horário operacional foi definido com base nesses períodos críticos. O perfil de carga dos E-buses, definido com base num modelo físico, resultou num consumo energético específico médio de 1,91 kWh/km ao nível do sistema de propulsão. A avaliação do recurso solar, baseiada no Ano Típico Meteorológico (TMY) extraído da PVGIS-SARA2, indicou uma média diária anual da irradiação global no plano horizontal (GHI) de 5,2 kWh/m² e uma irradiação global no plano inclinado (GTI) de 5,58 kWh/m² no ângulo ótimo de 29^{O}. Com base no perfil diário de carga e nos dados do PVGIS, foram avaliados dois cenários de dimensionamento de sistemas PV ligados à rede, com política de zero exportação e sob regime de autoconsumo estrito. O Cenário-1, dimensionado para satisfazer a totalidade da demanda diária ao longo do ano, gerou um excedente médio de cerca de 162 kWh/dia, justificando a integração de um Sistema de Armazenamento de Energia em Bateria (BESS). O Cenário-2, optimizado para corresponder à procura média anual, resultou num excedente líquido praticamente nulo, permitindo um elevado grau de autoconsumo e eliminando a necessidade de um BESS, com défices ocasionais supridos pela rede nacional. Os resultados demonstram que o carregamento de E-Buses com base em energia solar PV é tecnicamente viável e oferece benefícios ambientais significativos, incluindo a eliminação total das emissões de CO_2 no local sob fornecimento 100% PV e a remoção completa de emissões de NO_x e Material Particulado (PM) em todos os cenários de electrificação. Em suma, o estudo fornece um modelo replicável para a integração de energias renováveis e da electromobilidade como vectores-chave para a transição energética, tanto em Maputo como noutras cidades africanas.

Palavras-chave: Transição energética, Veículos elétricos, Mobilidade urbana, Autocarros eléctricos, Recurso solar

Table of Contents

Abstract vi
Resumo vii
LIST OF FIGURES xi
LIST OF TABLES xii
LIST OF ABBREVIATIONS AND ACRONYMS xiii
LIST OF SYMBOLS AND VARIABLES xv
Chapter 1 : INTRODUCTION 1
1.1- Contextualization 1
1.3- Aim and Objectives 4
1.3.1- Aim: 4
1.3.2- Objectives: 4
1.4- Spatial delimitation and Description of the study site 4
1.5- Maputo Bus Rapid Transit Project 5
Chapter 2 : THEORETICAL FRAMEWORK AND STATE OF THE ART 6
2.1- Solar Resource 6
2.1.1- Solar Energy and the Thermonuclear Fusion Reaction 6
2.1.2- Solar Radiation and Its Components 7
2.1.3- Solar Resource and the PV power Potential in Mozambique 9
2.2- PV Technology 9
2.2.1- PV Cells Modelling Methods 10
2.2.2- Effect of Meteorological Parameters on PV Module Performance 11
2.2.3- PV Cell Temperature Mathematical Modelling 11
2.2.4- PV Power dependence on irradiance and module temperature 13
2.2.5- Peak Sun Hours Concept in Solar PV Generation 14
2.2.6- Introduction to PV self-consumption 14
2.3- EV and Charging Technology: Overview 15
2.3.1-EV Categories and Powertrain topologies 16
2.3.2- EV Charging Technology 17
2.4- Solar energy integration with EV Charging infrastructure 19
2.4.1- Off-grid charging station configuration 19
2.4.2- On-grid Charging Station Configuration 20
2.4.3- Zero-export systems 21

2.5- State of the Art: Market Share, Challenges and Trends 22
2.5.1- PV Market Share, Challenges and Trends 22
2.5.2- EV Market Share, Challenges and Trends 24
2.5.3- E-Bus Charging Market Size, Challenges and Trends 26
Chapter 3 : MATERIALS AND METHODS 29
3.1- Case Study Description 29
3.2- Electric Buses load Profile 30
3.2.1- Physical Model 30
3.2.2- Physical Model Input parameters 31
3.2.3- Physical Model Input parameters 32
3.3- Solar Resource Profile 34
3.3.1 PVGIS-5.2 Spatial and Temporal Coverage and resolution 35
3.4- PV charging station Design and Sizing 36
3.4.1- Charging System Configuration and Operation Mode 36
3.4.2- Charger Sizing for Midday Energy Demand 36
3.4.3- PV System Sizing 37
Chapter 4 : RESULTS AND DISCUSSIONS 39
4.1- E-bus Energy Demand profile 39
4.1.1- E-buses Specific Energy demand 39
4.1.2- E-Buses Daily and Annual Energy Demand 40
4.2.1- Seasonal variation of Solar Radiation and Clearness Index 42
4.3- PV charging station Design and Sizing 44
4.3.1- PV System Energy Sizing 44
4.3.2- PVGIS Simulation for full-demand PV System 45
4.4- Energy and Environmental Implications 48
4.4.1- Energy Implications-Comparative Perspective 48
4.4.2- Environmental Implications of PV-Based Charging 49
Chapter 5 CONCLUSIONS AND RECOMMENDATIONS 50
5.1- Conclusions 50
5.2- Limitations 51
5.3- Recommendations for Future Research 51
CONFERENCE PAPER PRESENTATIONS 52
REFERENCES 55
APPENDIXES 60
Appendix A- Meteorological Data from PVGIS-SARAH2 (Maputo) 60
Appendix B- Daily bus operation at the battery efficiency level 61

Appendix C- Daily fleet operation at the charger efficiency level 61
ANNEXES 62
Annex A: Datasheet of VOLVO 7900 articulated E-bus 62
Annex B: Characteristic of the Charger considered in this study 65
Annex C: Physics model input parameters 66
Annex D: Characteristic of the PV modules considered in this study 67

LIST OF FIGURES

Figure 1.1- Global CO_2 emissions by transport mode [8] 1
Figure 1.2-Road transport energy consumption by energy source in Mozambique in 2022 [9] 2
Figure 1.3- Structure of the energy transition strategy in Mozambique 3
Figure 1.4-Map of Maputo Metropolitan Area and public transport network [13] 4
Figure 2.1- Life cycle of the sun [18] 6
Figure 2.2- Electromagnetic spectrum [19] 7
Figure 2.3- Disk-integrated solar spectra. Illustration based on [20] 8
Figure 2.4- Solar radiation components on a tilted surface (author) 8
Figure 2.5- a) Solar resource and (b) PV power potential map [22] 9
Figure 2.6- Electrical diagram of the single-diode model 10
Figure 2.7- Solar cell I-V Characteristics, under different conditions [18], [22], [24] 11
Figure 2.8- Derivation of the INOCT from the NOCT for various mounting configurations [26] 12
Figure 2.9- Effect of (a) irradiance and (b) temperature on different types of PV modules [27] 13
Figure 2.10- The effect of temperature and irradiance for a number [29] 14
Figure 2.11- Load, generation, and self-consumption in a building with on-site PV [30] 15
Figure 2.12- Trolleybus: (a) in 1882 and (b) modern version (Public domain image) 16
Figure 2.13- EV Categorization 16
Figure 2.14- Current E-bus charging methods [35] 17
Figure 2.15- Overview of EV charging levels [30] 18
Figure 2.16- Common connectors for E-buses 18
Figure 2.17- An overview of EV charging infrastructure [41] 19
Figure 2.18- An Off-grid PV-based EV charging station diagram 20
Figure 2.19- schematic illustration an on-grid charging station (Authors) 20
Figure 2.20- Zero export device [45] 21
Figure 2.21- A typical configuration of a zero-export EV charging system with a BESS 22
Figure 2.22- PV cells generations and their current developments [31] 22
Figure 2.23- Global PV Market Share by Technology [33] 23
Figure 2.24- Articulated urban buses: (a) Hybrid- Rome, (b) Full-electric- Berlin, 2025 (Author). 24
Figure 2.25- Electric bus market share (Forecast period: 2024-2030) [34] 25
Figure 2.26- An integrated system for E-Bus charging at Transdev's Capalaba Depot [36] 27
Figure 2.27- Global E-Bus charging station market size and scope [62] 28
Figure 2.28- Impact of E-Bus charges on the grid [29] 28
Figure 3.1- Map of the BRT N1 line [15] 29
Figure 3.2- Overall layout of (a) Maputo and (b) Zimpeto Terminals & Depots [15] 30
Figure 3.3- A schematic view of the longitudinal forces acting on the vehicle 30
Figure 3.4- Bus driving cycle diagram (author) 32
Figure 3.5- Daily bus operation cycle diagram (author) 32
Figure 3.6- The proposed BRT N1 road gradient map [74] 34
Figure 3.7- PVGIS-5.2 Spatial coverage [50] 35
Figure 3.8- An innovative energy system power flow 36
Figure 4.1- Simulated driving cycles in spatiotemporal domains: (a, b) 19 cycles; (c, d) one cycle 39
Figure 4.2- Route altimetry according elevation difference between the two terminals 39
Figure 4.3- Daily E-bus operation pattern 41
Figure 4.4- Temporal Evolution of the Solar Radiation and Clearness Index in Maputo 43
Figure 4.5- Seasonal variability of solar irradiance in Maputo 44
Figure 4.6- Monthly average PV output (a) 220.4kWp and (b) 181.5 kWp 47

Figure 4.7- Daily energy production and surplus: (a) 220.4kWp and (b) 181.5 kWp 48

LIST OF TABLES

Table 1.1: Location Outline of Stations and Terminals of the BRT N1 Line [16] 5
Table 2.1- X values for stand-off configuration [26] 12
Table 2.2- Charging Levels 18
Table 3.1- PV module specifications 35
Table 3.2- PVGIS-5.2 Spatial and Temporal Resolution 35
Table 3.3-EV Charger specification 37
Table 4.1- Energy Performance overview per trip, for a slope of 0.11% and 0.55% 40
Table 4.2- Daily Bus operation schedule 41
Table 4.3- Estimated daily and annual energy demand per E-bus 42
Table 4.4- Estimated daily and annual energy demand for three E-bus fleet 42
Table 4.5- Solar resources and climate data 43
Table 4.6- Load-Driven PV System Dimensioning 44
Table 4.7- PVGIS Input Parameters and Simulated Energy Output 46
Table 4.8- Description of Energy Supply Scenarios 49
Table 4.9- Comparative Emissions analysis across different scenarios 49

LIST OF ABBREVIATIONS AND ACRONYMS

AC	Alternating Current
AM	Air Mass
AM0	Extraterrestrial Spectrum
a-Si	Amorphous Silicon
BEV	Battery Electric Vehicle
BRT	Bus Rapid Transit
CCS	Combined Charging System
Cd	Drag coefficient of the Vehicle
CdTe	Cadmium Telluride
CHAdeMO	Charge de Move
CIGS	Copper Indium Gallium Selenide
CIS	Copper Indium Selenide
c-Si	Crystalline Silicon
ETS	Energy Transition Strategy
EV	Electric Vehicle
EVCS	Electric Vehicle Charging Station
FCEV	Fuel cell Electric Vehicle
GHI	Global Horizontal Irradiance
GHG	Greenhouse gases
GCR	Ground Coverage Ratio
GTI	Global Tilted Irradiance
HEV	Hybrid Electric Vehicle
ICEV	Internal Combustion Engine Vehicle
IEC	International Electrotechnical Commission
iHOGA	Improved Hybrid Optimization by Genetic Algorithms
MMA	Maputo Metropolitan Area
Mpt	Maputo Terminal
NO_x	Nitrogen Oxides
OsmAnd.	OpenStreetMap Automated Navigation Direction

OSM	OpenStreetMap
PHEV	Plug-in Hybrid Electric Vehicle
PM	Particulate Matter
PR	Performance Ratio
PV	Photovoltaic
PVGIS	Photovoltaic Geographical Information System
RES	Renewable Energy Sources
SAE	Society of Automotive Engineers
SAM	System Advisor Model
SC	Self-Consumption
SOC	State of Charge
STC	Standard Test Conditions
TMY	Typical Meteorological Year
V2G	Vehicle-to-Grid
WTW	Well-To-Whell
ZED	Zero Export Device
Zmpt	Zimpeto Terminal

LIST OF SYMBOLS AND VARIABLES

A_f	Frontal Area of the Vehicle *(m^2)*
c	Speed of light *(m/s)*
C_d	Aerodynamic drag coefficient of the vehicle
C_r	Rolling resistance coefficient
δ	Inertia factor of rotating components
E_g	Bandgap Energy
f	Frequency *(s^{-1})*
F_{aero}	Aerodynamic drag force *(N)*
F_{gX}	Track gradient resistance force longitudinal gravity component *(N)*
F_r	Rolling resistance force *(N)*
F_t	Tractive force *(N)*
g	Gravitational acceleration*(m/s^2)*
G_M	Solar radiation striking the PV array (W/m^2)
G_T	Global Tilted Irradiance (W/m^2)
$G_{T,b}$	Beam or Direct Irradiance on a Tilted Surface (W/m^2)
$G_{T,d}$	Diffuse Irradiance on a Tilted Surface (W/m^2)
$G_{T,r}$	Reflected Irradiance on a Tilted Surface (W/m^2)
H_0	Extraterrestrial Radiation (kWh/m^2)
H_b	Direct or Beam Radiation (kWh/m^2)
H_d	Diffuse Radiation (kWh/m^2)
h	Planck's constant *(J.s)*
I_0	Diode reverse saturation current *(A)*
I_L	Photocurrent *(A)*
I_{SC}	Short Circuit Current *(A)*
K	Boltzmann's constant *(J/K)*
λ	Wavelength *(m)*
M	Total mass of the vehicle including load (kg)

N	Diode ideality factor
N_S	Number of cells in series
P_{aux}	Auxiliary Power (W)
q	Electric Charge
R_P	Shunt resistance
R_S	Series resistance
T_a	Ambient air temperature
T_C	Cell temperature
$T_{C,NOCT}$	Installed Nominal Operating Cell Temperature
$T\alpha$	Effective transmittance-absorptance product
V_{oc}	Open Circuit Voltage
w	Wind speed
ρ	Air density

Chapter 1 : INTRODUCTION

1.1- Contextualization

The current global energy landscape is undergoing profound transformations which underscores the urgent need to address climate changes and shift from fossil-based systems to sustainable energy models. Our planet is becoming increasingly populated and polluted, which intensifies environmental and energy-related pressures in urban areas. Between 1950 and 2020, the global population has tripled, the African population has sextupled, and the Mozambican population has quintupled [1], [2], [3]. In urban areas, the global population increased approximately sixfold, while Mozambique experienced a 50-fold growth in urban concentration, with the highest density in Maputo [4], [5], [6].

In the globally context, the transport remains one of the most fossil fuel–dependent sectors, with oil providing over 90% of its energy [7]. It contributes about 25% of global CO_2 emissions, with road transport alone responsible for nearly 75% [8]. These emissions, along with NO_x and Particulate Matter (PM), accelerate climate change, degrade air quality, and endanger public health. As shown in Figure 1.1, CO_2 emissions by transport mode clearly reflect the dominance of road transport.

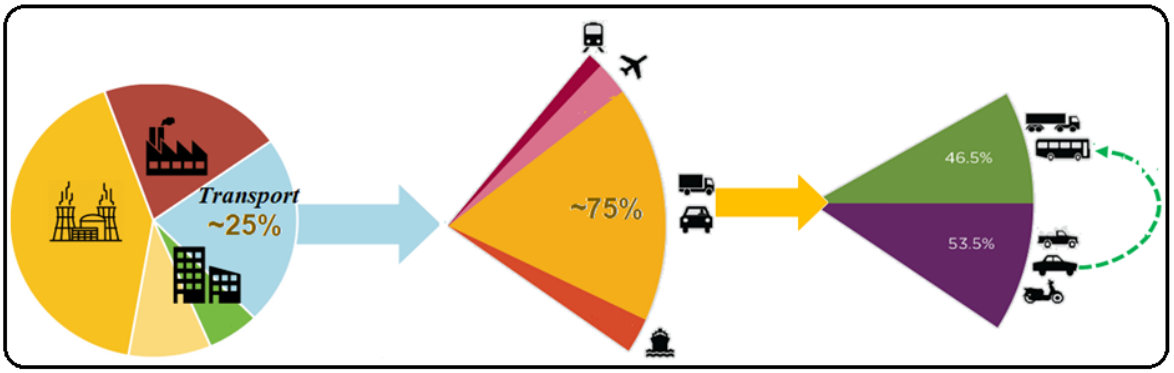


Figure 1.1- Global CO_2 emissions by transport mode. Adapted from [8]

This global pattern is strongly reflected in Mozambique, where the transport sector remains overwhelmingly reliant on fossil fuels. In 2022, road transport energy consumption was almost entirely reliant on fossil fuels, with oil products accounted for 55,443 terajoules of total demand, while natural gas contributed 152 terajoules, representing only 0.27% of total consumption. Renewable sources registered no usage in the sector, as shown in Figure 1.2 [9]. Such dependence underscores the limited diversification of the national transport energy mix and highlights the urgent need for cleaner alternatives in urban mobility. This challenge is

further exacerbated by rapid motorisation: by 2024, the number of registered vehicles had risen to approximately 528,179 in Maputo City and further 457,546 in the surrounding provincial area [10], significantly placing strain on urban infrastructure, energy systems, and the environment.

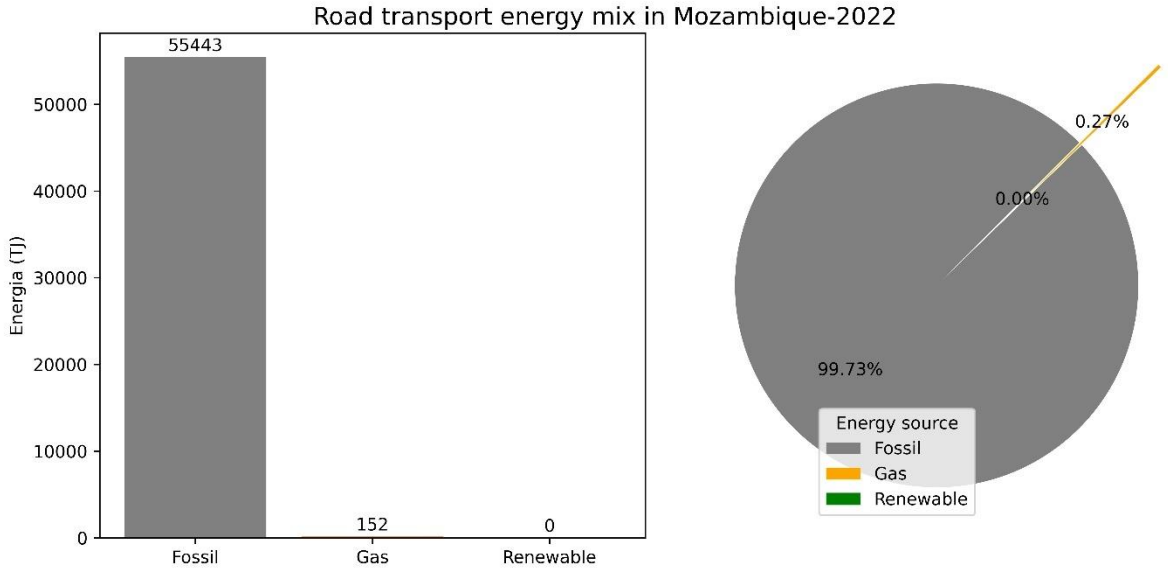


Figure 1.2-Road transport energy consumption by energy source in Mozambique in 2022 [9]

To address these pressures, Mozambique has defined an Energy Transition Strategy (ETS), structured around four pillars and fourteen priority programs as shown in the Figure 1.3. The fourth pillar emphasizes the adoption of electric mobility and collective transport, addressing both energy efficiency and environmental sustainability [11].

The country benefits from an abundance of solar energy resources, with annual potential estimated at 1.49 million GWh and average daily solar irradiation of 5.7 kWh/m², ranging between 4 and 7 kWh/m² across its territory [12], [13]. Harnessing these resources for e-bus infrastructure allows the alignment of urban mobility needs with renewable energy utilization, providing a pathway to reduce fossil fuel consumption and urban emissions while ensuring reliable energy supply for transport. The present study focuses on the proposed Bus Rapid Transit (BRT) Line N1 in the Maputo Metropolitan Area (MMA), with the integration of Photovoltaic (PV) system into the charging infrastructure for E-buses. The expectation is a decreased reliance on fossil fuels and, consequently, a reduction in CO_2 emissions, accompanied by the mitigation of both air and noise pollution.

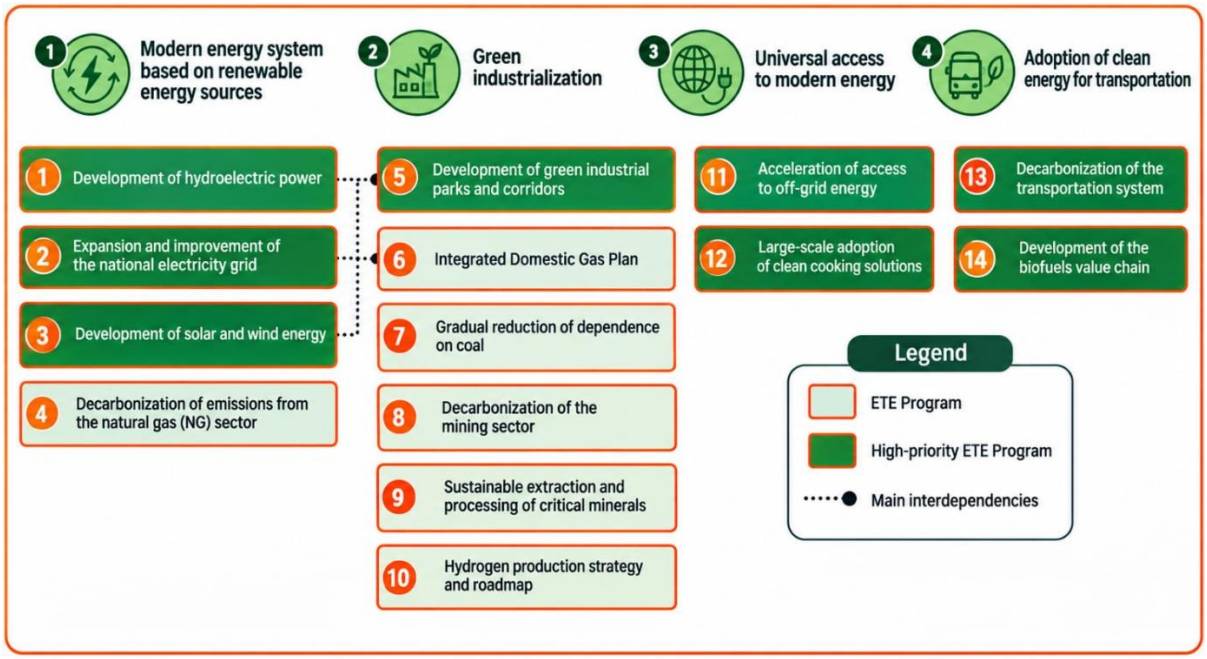


Figure 1.3- Structure of the energy transition strategy in Mozambique [11]

1.2- Justification

E-buses designed for mass transit systems have the capacity to accommodate a significantly larger number of passengers, making them pivotal contributors to emissions reduction and traffic decongestion in densely populated urban areas. In the international context, this research aligns with the agenda of the United Nations (UN), specifically within the scope of Sustainable Development Goals (SDGs) 7, 11, and consequently 13, which advocates for a substantial increase in the share of renewable energies in the global energy matrix, an access to sustainable and safe transport systems for all, notably by expanding public transport, a promotion of investments in energy infrastructure and clean energy technologies, an expansion of infrastructure and technological modernization for the provision of modern and sustainable energy services, particularly in less developed countries such as Mozambique by 2030. In the national context, the research is based on the fourth pillar of the ETS in Mozambique, which advocates for the shift from a petroleum-dependent transport system and private vehicles to Electric Vehicles (EVs) and public transport, which decarbonization of the transport system is one of the high priority programmes within this framework [11]. From the perspective of renewable energy resources, Mozambique disposes abundant solar resources, with annual potential estimated at 1.49 million GWh and average daily solar irradiation of 5.7 kWh/m², ranging between approximately 4 and 7 kWh/m² across its territory [12], [13].

1.3- Aim and Objectives

1.3.1- Aim:

The aim of this study is to design and evaluate a grid-connected, zero-export, PV-integrated e-bus charging system for the proposed BRT N1 line, within the Maputo Metropolitan Area

1.3.2- Objectives:

- To estimate the load profile of electric city buses to manage the proposed BRT N1 line;
- To assess the solar resource profile in the Maputo Metropolitan area;
- To size a grid-connected PV system at Maputo terminal and deport.

1.4- Spatial delimitation and Description of the study site

The study is limited to the BRT Line-2 (Zimpeto–Benfica–Brigada-Maputo Station) in the MMA. The MMA includes the municipalities of Maputo, Matola, Boane and the district of Marracuene, in southern Mozambique. The predominant climate in this region is tropical, classified as Aw according to the Köppen-Geiger climate classification. The city has two main seasons: a hot and rainy season from October to March, and a cold and dry season from April to September. Maputo Terminal & Depot is located in Maputo downtown, approximately 10 m above sea level, while the Zimpeto Terminals & Depots is located about 19.1 km from the city center at an elevation of 31 m above sea level.

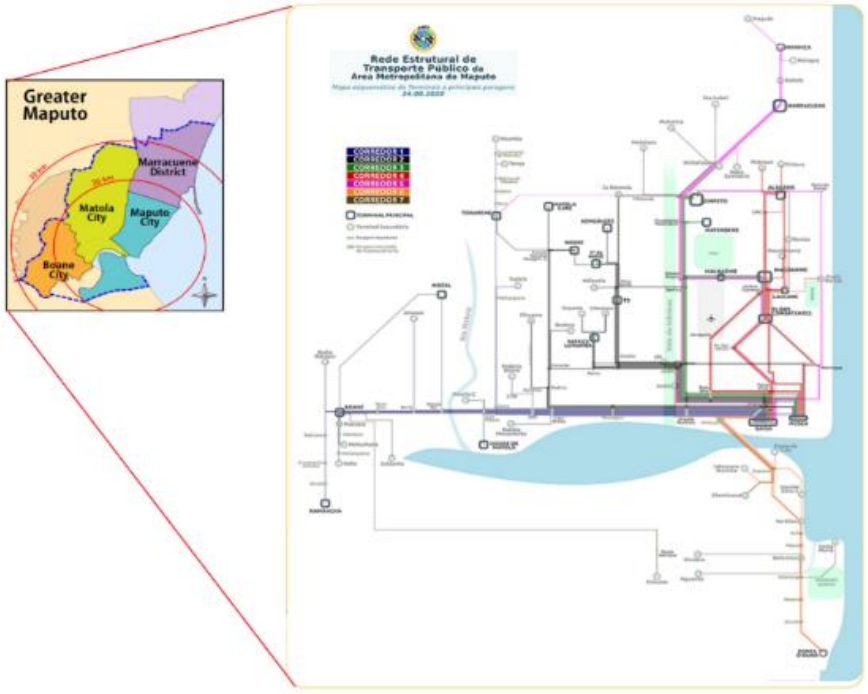


Figure 1.4-Map of Maputo Metropolitan Area and public transport network [13]

1.5- Maputo Bus Rapid Transit Project

BRT is a bus-based transit system that combines segregated bus lane and bus priority at intersections to achieve high capacity, speed, and service quality at a lower cost. Buses operate on tracks segregated from other, enhancing efficiency and service reliability [14], [15].

In the context of the development program for Maputo, adopted by the government of Mozambique, plans were made for a BRT system for the city. However, due to the lack of a concrete and long-term vision for urban transport, among other reasons, the government of Mozambique requested assistance from the Japanese government. This led to the production of a comprehensive master plan for urban transport in the Greater Maputo region, with a target year of 2035. Within this framework, the Japan International Cooperation Agency (JICA) presented three alternative routes for the BRT system, namely:

Route N1: From Zimpeto to CFM Station, via Brigada;

Route East Maputo: From Magoanine to the CFM Station (downtown), via Praça dos Combatentes and with a connection to the Natural History Museum Terminal;

Route Matola – Maputo: Via N2 and N4 to the CFM Station.

In parallel, an implementation plan was developed for high-priority projects, among which the BRT corridor N1 was selected for a pre-feasibility study.

According to JICA [16], on the BRT N1 line, which comprises a 19.1 km extension, there are 16 stations and three proposed terminals. The outline of the station and terminal locations is presented in Table 1.1 and illustrated on the map in Figure 1.3.

Table 1.1: Location Outline of Stations and Terminals of the BRT N1 Line [16]

Section	Length	Terminal/Number of Stations
Maputo Station-Brigada	3.8 km	3 stations, I terminal
Brigada-Missão Roque	8.7 km	9 stations, I terminal
Missão Roque-Zimpeto	6.6 km	4 stations, I terminal
Total	19.1 km	16 stations, 3 terminals

Chapter 2 : THEORETICAL FRAMEWORK AND STATE OF THE ART

2.1- Solar Resource

The sun is a stable main sequence star, and therefore, a composition of intensely hot gaseous matter, with a predominance of hydrogen (about 73% of its mass) and helium (aproximately 25% of its mass). Its estimated age is 4.5 billion years, and it is expected to remain in this phase for another 4 to 5 billion years before entering the next stage of its evolution, the burning of helium [17]. Figure 2.1 below illustrates the life cycle of the sun, from its formation to its eventual transformation.

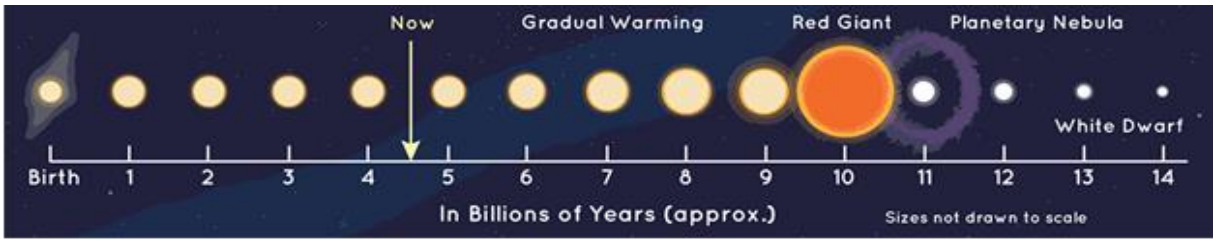


Figure 2.1- Life cycle of the sun [18]

2.1.1- Solar Energy and the Thermonuclear Fusion Reaction

In Physics, the concept of Energy can be defined as the capacity of a physical system to perform work, manifesting itself in different ways. As Einstein famously stated, "Everything in the universe, except space itself, is just energy." Wherever we are, there is never a true shortage of energy; rather, the global challenge is the shortage of technology and mechanisms to convert the energy that is all around us, into usable forms [19]. And according to the principle of conservation (attributed to Lavoisier), energy cannot be created or destroyed, only transformed from one form into another.

When it comes to the sun, energy transformation occurs through thermonuclear fusion, specifically the proton-proton cycle. This process involves the fusion of four hydrogen nuclei to form a single helium nucleus, producing two positrons, two neutrinos, and a specific amount of energy, as shown in Equation 2.1 [20]. In this reaction, mass is converted into energy in accordance with Einstein's formula, Equation 2.2, resulting in an energy release of $\Delta E =$ 24.687 MeV.

$$4{}_1^1P \rightarrow {}_2^4\alpha + 2e^+ + \nu_e + \Delta E \quad (2.1)$$

$$\Delta E = \Delta m C^2 \quad (2.2)$$

Taking into account the electrons in the atomic shell which contribute with a radiative energy, which is four times the equivalent mass of an electron of 2.044 MeV, the total energy released during the thermonuclear fusion reaction amounts 26.731 MeV. These results, considering the expected lifetime of the sun, clearly demonstrate that the Sun is the most abundant renewable energy source, capable to meet the Earth's energy demand in a sustainable way.

2.1.2- Solar Radiation and Its Components

Solar radiation is the primary source of energy, from which all other forms of energy utilized on Earth ultimately derive. This electromagnetic energy propagates through space as waves, travelling at a velocity of 3×10^8 m/s. The electromagnetic spectrum illustrated in Figure 2.10, is formed by the set of all wavelengths, ranging from 10^{-10} cm (gamma rays) to approximately 10^7 cm (long radio waves). Each wavelength corresponds to a specific frequency and energy, as described by Equation (2.3).

$$f = C/\lambda \text{ and } E = hf \tag{2.3}$$

In this set of wavelengths, only the wavelength range between approximately 0.38 μm and 0.78 μm, equivalent to an energy range of approximately 1.59 eV to 3.26 eV, can be detected by the human eye.

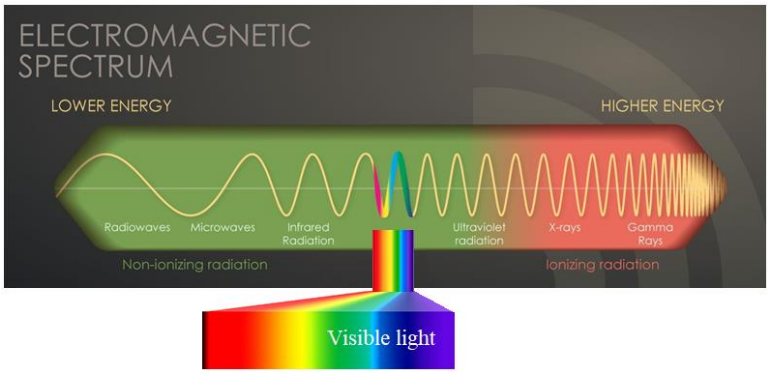


Figure 2.2- Electromagnetic spectrum [19]

As mentioned in the previous section, the Sun generates its energy from thermonuclear fusion reaction. This energy is transferred out from the Sun's core to its surface and then radiated into space [21]. The portion of this radiation that reaches the top of the Earth's atmosphere is referred to as extraterrestrial radiation (H_0). Its spectral distribution, illustrated in Figure 2.3, varies slightly with solar activity and depends on factors such as latitude, solar declination and hour angle, all of which are governed by the Sun–Earth geometric relationship.

As solar irradiation passes through the atmosphere it is reduced due to absorption by atmospheric gases, such as O_2, O_3, CO_2, and H_2O, due to Mie scattering and Rayleigh scattering [20]. The amount of sunlight either absorbed or scattered depends on the length of path through the atmosphere. This path length is typically compared with a vertical path directly to sea level, which is referred to as air mass (AM). Due to absorption effects, approximately 7% of the extraterrestrial spectrum (AM0) falls within the ultraviolet range, 47% within the visible range, and 46% in the infrared. Rayleigh scattering occurs when molecular air particles are smaller than the wavelength of light, while Mie scattering is caused by larger particles such as dust and atmospheric pollutants [20]. 21

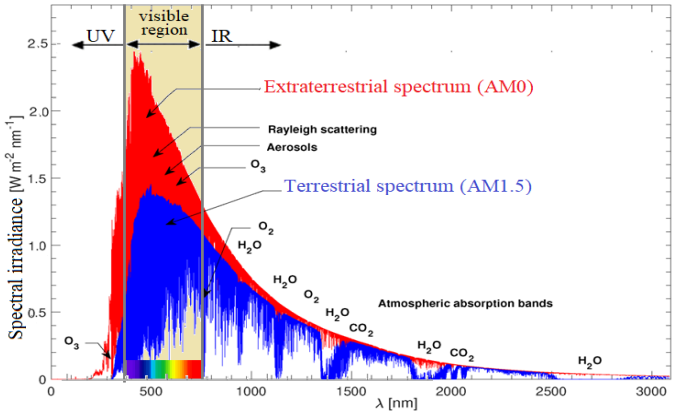


Figure 2.3- Disk-integrated solar spectra. Illustration based on [20]

Solar radiation that penetrates the Earth's atmosphere is referred as terrestrial radiation or solar global radiation. When it reaches the surface without scattering it is called direct or beam radiation (H_b) and when scattered through the atmosphere is called diffuse radiation (H_d). Beneath the atmosphere, the hourly total irradiance incident on a tilted surface (G_T), as shown in Figure 2.4 is composed of direct or beam ($G_{T,b}$), sky diffuse ($G_{T,d}$) and ground reflected (G_r) components, and calculated as Equation (2.4) [20], [22]:

$$G_T = G_{T,b} + G_{T,d} + G_{T,r} \tag{2.4}$$

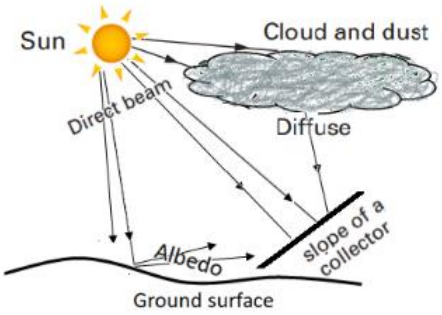


Figure 2.4- Solar radiation components on a tilted surface (author)

2.1.3- Solar Resource and the PV power Potential in Mozambique

The solar resource potential will vary from location to location according to seasonal cloudiness and solar position. According to the Global Solar Atlas, the long-term average of global horizontal irradiation on daily basis varies from 2.2 to 7.4 kWh/m^2 worldwide.

In Mozambique, the annual incident solar radiation, evenly distributed across the country is around 1.49 million GWh, with an annual daily average of around 5.7 kWh/m^2 [13], which can vary between approximately 4.5 and 7 kWh/m^2 throughout the country. Figure 2.5a illustrates the spatial distribution of global horizontal irradiance across the country while Figure 2.5b shows the spatial variability of the potential energy yield on both daily and annual basis, based on a specific PV technology.

Despite the high levels of incident solar radiation observed throughout Mozambique, the rainfall regime which intensifies from south to north, significantly influences the spatial distribution and availability of solar energy, particularly in the interior regions [12].

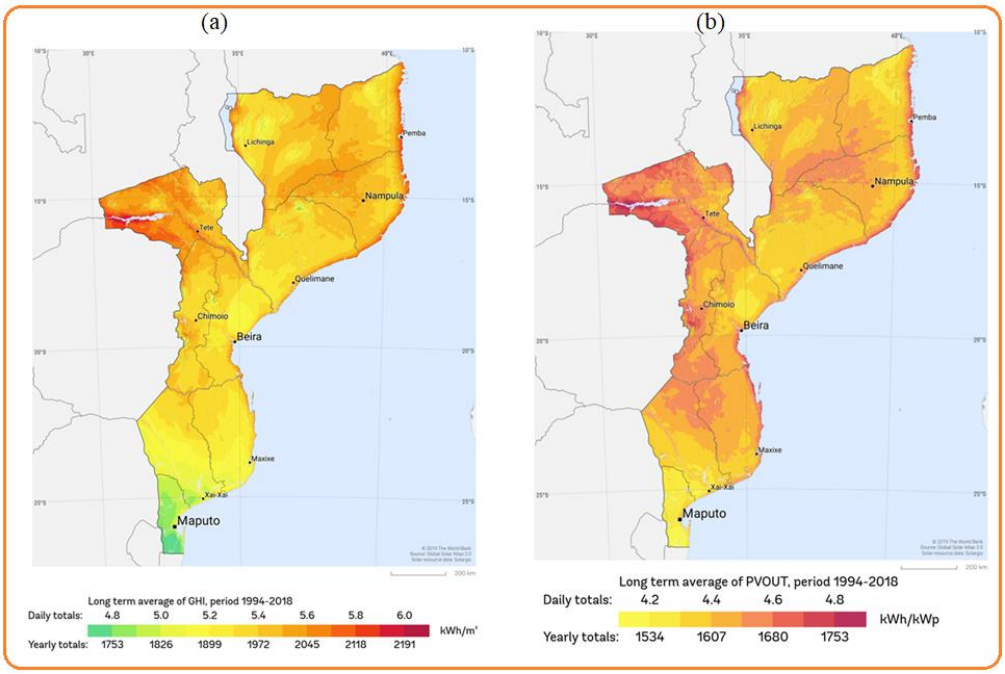


Figure 2.5- a) Solar resource and (b) PV power potential map [23]

2.2- PV Technology

PV Technology is intrinsically linked with the development of quantum mechanics as solar cells are semiconductors that respond to discrete packets of light or quanta, converting part of the incident solar radiation directly into electrical energy [21], [24]. Building upon this quantum-based mechanism, solar PV energy has become one of the most significant and

rapidly expanding renewable energy technologies worldwide. PV systems operate by exploiting the photovoltaic effect to convert solar irradiance into usable electrical power and typically comprise solar modules, power inverters, mounting structures, and, in many cases, energy storage solutions. The performance and efficiency of PV generation are determined by multiple factors, including solar irradiance intensity, ambient temperature, module orientation, tilt angle, and the intrinsic properties of the photovoltaic technology employed.

2.2.1- PV Cells Modelling Methods

Any PV device can be modelled using the equivalent circuit model. These electrical models with the ability to predict *I-V* characteristics of a PV cell or module under the working environment other than Standard Testing Conditions (STC), are predictive performance tools that allow PV system designers to understand, optimize and design PV power generation systems. Among several existing models, the single diode, as illustrated in the Figure 2.6 is generally considered for his simplicity and accuracy.

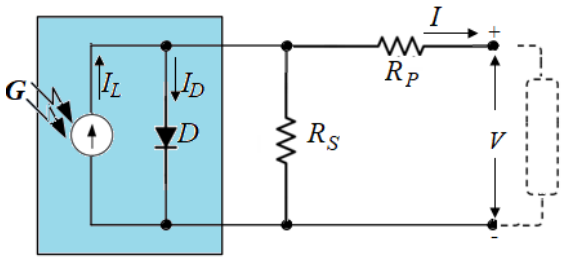


Figure 2.6- Electrical diagram of the single-diode model

PV cells are typically modelled using diodes due to their semiconductor composition. The electrical power generation is represented by a current source, while energy losses within the PV cells are accounted for by series and parallel resistances, as illustrated in Figure 2.6. At a fixed temperature and solar radiation, the *I-V* characteristic of this model is given by Equation (2.5).

$$I = I_L - I_O\left[\left(exp\frac{V+IR_S}{\frac{nkT_cN_S}{q}} - 1\right)\right] - \frac{V+IR_S}{R_P} \qquad (2.5)$$

The mathematical model of the PV Cell above, which is a single-Diod model, requires that five parameters be known, namely: the photo-current (I_L), the diode reverse saturation current (Io), the series resistance (Rs), the shunt resistance R_P, and the diode ideality factor (n). According to Duffie, Beckman, & Blair [21], n equal to 1 for an ideal diode and typically between 1 and 2 for real diodes. k is Boltzmann's constant (1.381×10^{-23} J/K), T is the cell temperature (to be estimated from mathematical models), Ns is the number of cells in series and q is the electronic charge (1.602×10^{-19} C).

2.2.2- Effect of Meteorological Parameters on PV Module Performance

Among other factors, the behaviour of a PV System is greatly influenced by the solar irradiation availability and temperature. When designing a PV System, an accurate model of the solar cells will be required to be able to study it under ideal conditions.

a) Irradiance

According to Buni, Al-Walie, & Al-Asadi [25], in their experimental study investigating the relationship between solar radiation, current, voltage and the efficiency of solar panels, an increase in solar radiation leads to an increase in output current, which improves the performance of a solar panel. Figure 2.7a illustrates the Influence of the Irradiance on the I-V Characteristics of a Solar Cell, at a fixed temperature level.

b) Temperature

The Short Circuit Current (I_{sc}) increases slightly with temperature, since the bandgap energy (E_g) decreases, and more photons have enough energy to create electron-hole (e-h) pairs. However, this is a small effect. The main effect of increasing temperature for silicon solar cells is a reduction in Open Circuit Voltage (V_{oc}), the fill factor and hence the cell output [24]. These effects are illustrated in Figure 2.7b, at a fixed radiation level.

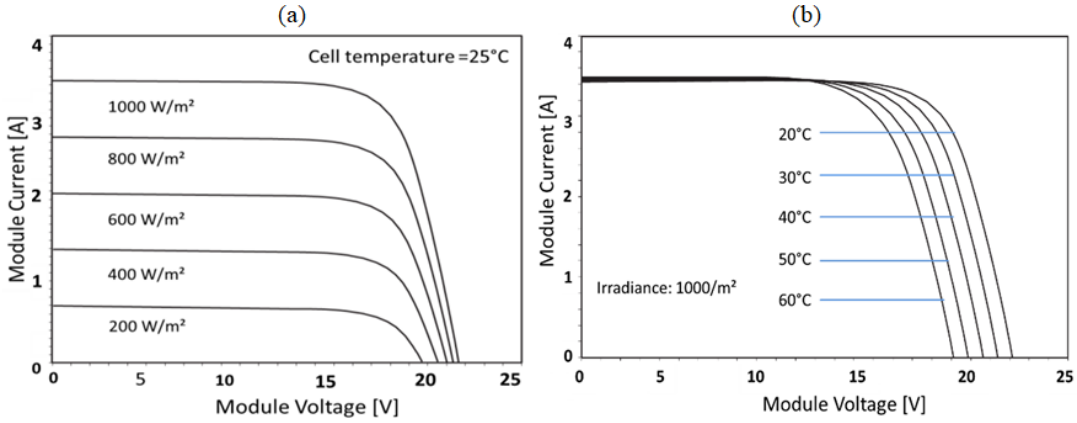


Figure 2.7- Solar cell I-V Characteristics, under different conditions [18], [22], [24]

2.2.3- PV Cell Temperature Mathematical Modelling

Experiments show that the performance of PV cells decreases dramatically as the temperature rises, Figure 2.9. Therefore, when sizing a solar PV system, especially in cities like Maputo and Tete where temperatures are relatively high, temperature is one of the parameters that should be considered as relevant. Unlike solar radiation, which can be easily estimated through measurements, the temperature of a solar cell inside a photovoltaic module is much more difficult to assess, which is why mathematical models are needed to estimate it correctly. There

are several models in the literature, from steady to dynamic state but each one gives different results. However, the conclusion is that the models should be used according to the configuration of the module and the region.

a) Installed Nominal Operating Cell Temperature Model

when the PV module is installed in a confined space such as a rooftop or building integration, Equation 2.4 can lead to significant errors. Furthermore, the same equation cannot be applied for PV modules that have an absorber plate with circulating fluid and insulation [26]. Fuentes [27] presents a model in which he considers the mounting configuration and, in the same model, the author verified that the Installed Nominal Operating Cell Temperature (INOCT) is −1 to 11 ˚C higher than the Nominal Operating Cell Temperature (NOCT) temperature when the PV is installed in stand-off configuration on the roof, as shown in Figure 2.8.

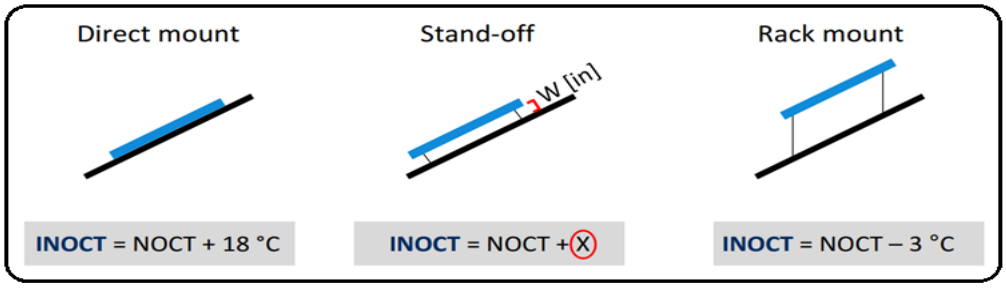


Figure 2.8- Derivation of the INOCT from the NOCT for various mounting configurations [26]

Table 2.1- X values for stand-off configuration [26]

X (^{0}C)	W (cm)
-1	15.24
2	7.62
11	2.54

b) Simple Modell

It is a steady state model which Ignore the mounting configuration and the wind speed

$$T_C = T_a + \left(T_{C,NOCT} - T_{a,NOCT}\right)\frac{G_T}{G_{T,NOCT}} \qquad 2.6$$

c) Duffie, Beckman Model

The Equation (2.7) presented by Duffie, Beckman and Blair [21] is a steady state model which estimates the temperature of the PV module, considering the convection coefficient, the solar radiation incident on the PV array and the wind speed.

$$T_C = T_a + \left(T_{C,INOCT} - T_{a,INOCT}\right)\frac{G_M}{G_{T,INOCT}} \cdot \frac{9.5}{5.7+3.8w}\left(1 - \frac{\eta_C}{\tau\alpha}\right) \qquad (2.7)$$

In expression 2.7, the product *(τα)* is not generally known but, according to Duffie, Beckman and Blair [21], an estimate of 0.9 can be used without serious error since the term *ηc/(τα)* is small compared to unity. η_C is the efficiency of the module in converting incident radiation into electrical energy; T_C is the cell temperature (to be calculated); T_a is the ambient air temperature (from database); $T_{C,INOCT}$ is the INOCT, which is provided by the manufacturer, calculated taking into account the mounting configurations; G_M is the solar radiation striking the PV array (to be calculated) and *w* is the local wind speed (to be measured).

2.2.4- PV Power dependence on irradiance and module temperature

The efficiency of PV modules depends on the temperature of the module and on the solar irradiance. Generally, the efficiency decreases with increasing temperature, and the strength of this effect depends on the PV technology as shown in Figure 2.9. For most module types, the efficiency is nearly constant for irradiances from about 400W/m^2 to at least 1000W/m^2 (for constant module temperature), but at lower irradiance the efficiency tends to decrease. Since the standard test conditions measure module power at high irradiance (1000W/m^2) and fairly low temperature (25°C), the overall result is that for most places the average module efficiency is a bit lower than the efficiency measured at the factory. To account for these environmental effects, the actual DC output power (P_{DC}) of a PV module can be estimated using the Equation (2.8):

$$P_{DC} = P_{STC}\left(\frac{G_M}{G_{MSTC}}\right)[1 + \alpha(T_C - T_{STC})] \qquad (2.8)$$

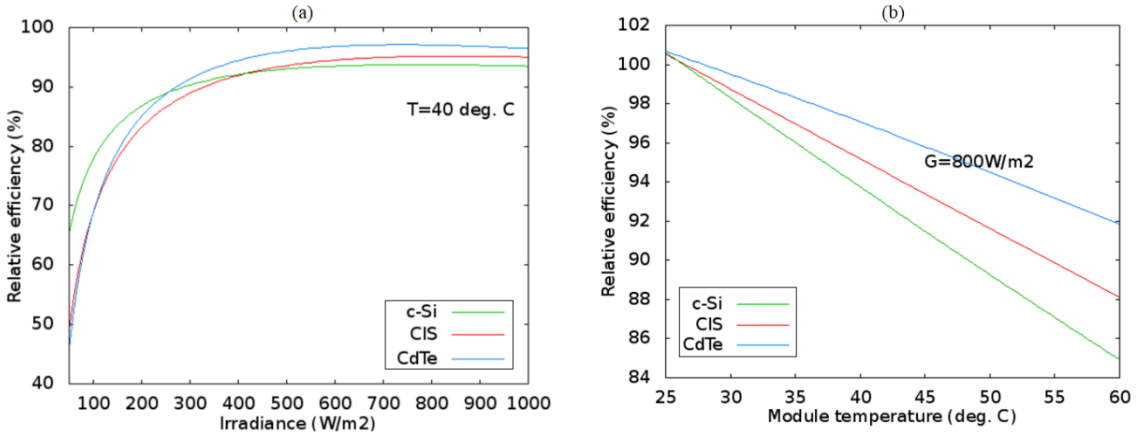


Figure 2.9- Effect of (a) irradiance and (b) temperature on different types of PV modules [27]

2.2.5- Peak Sun Hours Concept in Solar PV Generation

In PV solar generation, the concept of Peak Sun Hours (PSH) is employed to simplify the estimation of daily solar energy production, given the linear relationship between energy output and hourly irradiance. PSH standardizes the variation in solar irradiance by expressing the total daily solar energy received as an equivalent number of hours at a constant irradiance of 1 kW/m^2. This metric helps to express the accumulated energy over a 24-hour period in a standardized manner [22], [28], [29]. To illustrate how PSH is calculated, consider a scenario where irradiance levels over the day correspond to energy values of 6 kWh/m^2, 2.5 kWh/m^2, and 1.0 kWh/m^2. The PSH in each case represents the number of hours during which a constant irradiance of 1 kW/m^2 would yield the same total energy [29] . Figure 2.10 provides a visual example of this calculation, demonstrating how varying irradiance levels are converted into peak sun hour.

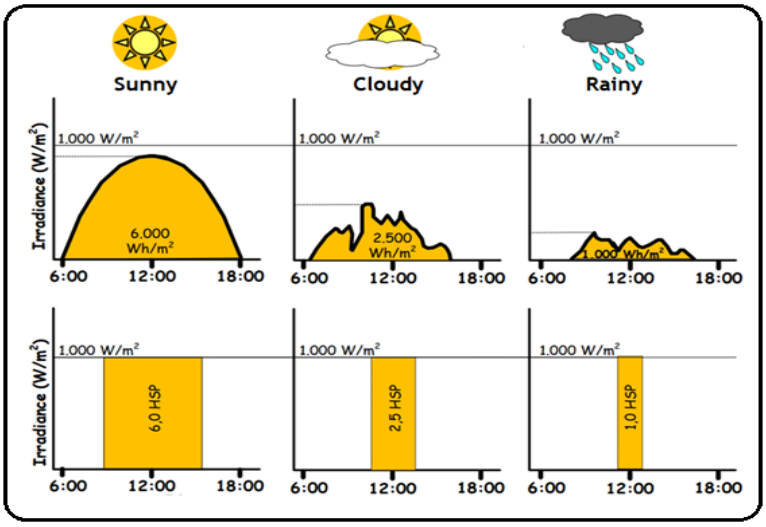


Figure 2.10- The effect of temperature and irradiance for a number [29]

2.2.6- Introduction to PV self-consumption

Self-consumption (SC) is defined as the fraction of the self-consumed PV energy to the total production, while self-sufficiency (SS) is defined as the fraction of the self-consumed PV electricity to the total consumption [30], [31]. Based on the illustration in Figure 2.11, the SC can be defined as Equation (2.9).

Within the scope of self-consumption with connection to the electricity grid, there are two types of self-consumption. The first is with surpluses, in which the surplus energy is exported to the electricity grid, and the second is without surpluses, in which it is not allowed to inject the surplus energy into the electricity grid. This second type results in an undersized, or a reduced capacity factor of the PVS which brings less contribution to clean energy than self-consumption

with surpluses [32]. To increase photovoltaic self-consumption there are different technologies. The two major ones are energy storage, mainly through batteries, and active load shifting, which is an important part of the concept demand-side management (DSM).

$$SC = \frac{C}{B+C} \tag{2.9}$$

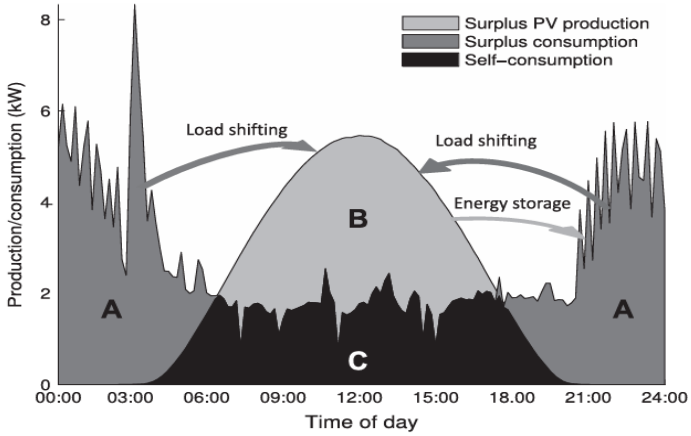


Figure 2.11- Load, generation, and self-consumption in a building with on-site PV [30]

2.3- EV and Charging Technology: Overview

The technology of EVs is closely linked to the development of electromagnetism. In the early 19th century, Volta demonstrated the potential for chemical energy storage, and in 1821, Faraday, utilizing Volta's batteries, established the fundamental principles of electric motors and generators, marking the beginning of the first phase in the development of EVs [33]. In 1882, Siemens developed the trolleybuses, powered by electric motors fed by overhead cables, which quickly became an alternative in many cities [33], [34].

With the invention of the electric starter motor in 1912, interest in EVs lessened. However, the oil crises of the 1970s renewed interest in the development of EVs. Subsequently, E-Buses have evolved into various configurations, as will be detailed in the following section. An example of early and modern trolleybus designs is illustrated in Figure 2.12.

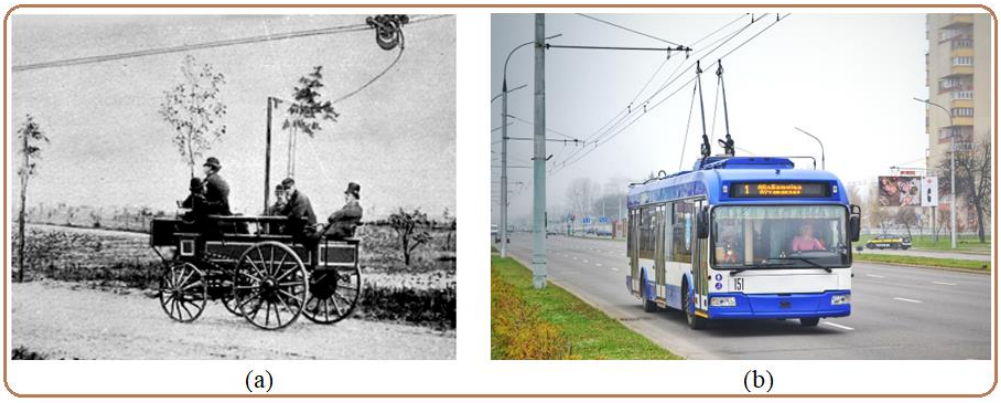


Figure 2.12- Trolleybus: (a) in 1882 and (b) modern version (Public domain image)

2.3.1-EV Categories and Powertrain topologies

In terms of categorization, EVs are classified into Hybrid EVs (HEVs), Plug-in EVs, which include Plug-in Hybrid EVs (PHEVs) and Battery EVs (BEVs), and Fuel cell EVs (FCEVs), as illustrated in Figure 2.13. BEVs and PHEVs are charged by plugging them into an external electric power source, while FCEVs require hydrogen distribution infrastructure. HEVs, on the other hand, obtain electrical energy internally through regenerative braking and through the internal combustion engine, depending on their powertrain topologies, which can be classified as parallel, series, or series-parallel [35]. The charging of plug-in EVs is enabled by different charging technologies, which are described in the next subsection.

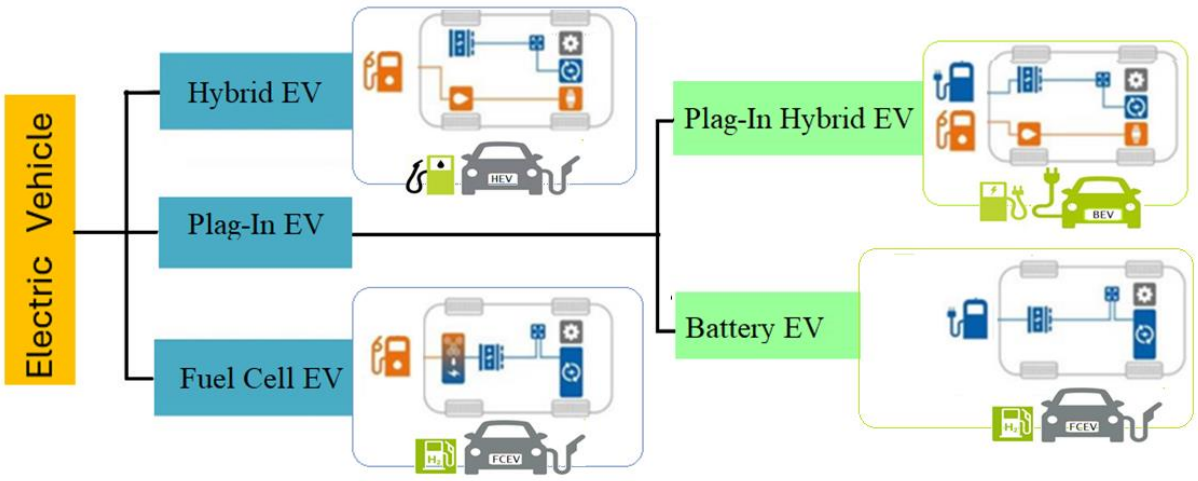


Figure 2.13- EV Categorization

2.3.2- EV Charging Technology

Battery swapping, conductive charging and wireless charging are the three methods by which EVs are charged. Among these, conductive charging is the most commonly employed for commercial EVs [36]. In the context of E-buses, three primary charging modes are typically used: Depot charging, en-route charging, and in-motion charging. These three charging modes are further subcategorized into specific techniques such as plug-in, pantograph, battery swapping, wireless, and catenary charging, as illustrated in Figure 2.14. In the figure, yellow boxes represent conductive charging techniques, while green boxes indicate inductive charging methods [37].

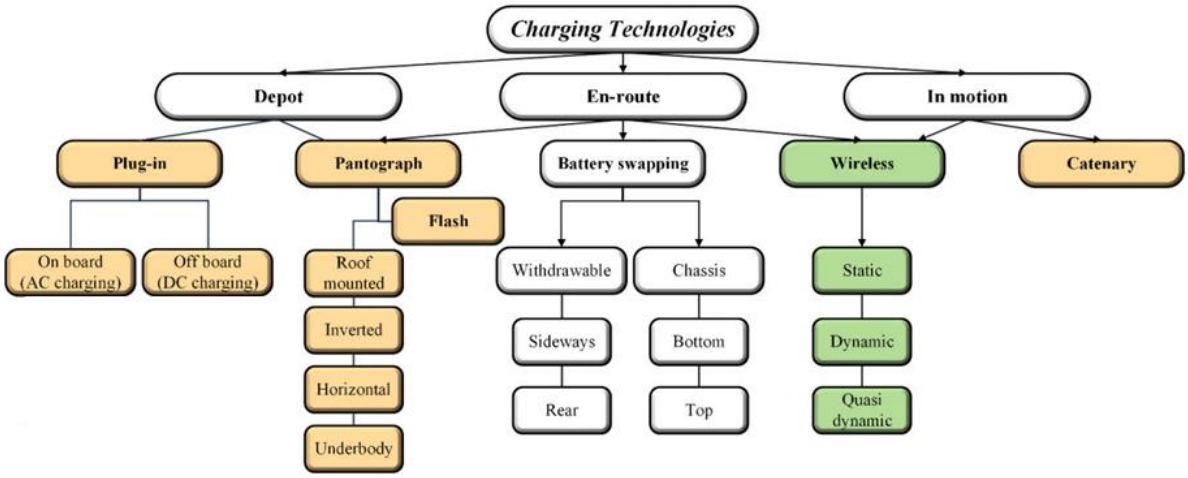


Figure 2.14- Current E-bus charging methods [35]

According to the International Electrotechnical Commission (IEC 61851-1) standards there are four different charging modes, each defined by specific voltage, current, and charging time characteristics. Additionally, the Society of Automotive Engineers (SAE J1772) defines three charging levels as summarized in the Table 2.2 and illustrated in Figure 2.15, which correspond to different power capacities and charging speeds [36]. Mode 4 is a special case in which the conversion from AC-to-DC occurs within the charging station itself, providing DC charging to the vehicle. This setup minimizes energy losses and slowdowns associated with onboard conversion system. For electric buses, connectivity standards vary depending on the manufacturer. The three most common DC charging interfaces are CHAdeMO, CCS, and GB/T, as illustrated in Figure 2.16.

Table 2.2- Charging Levels

Charging Level/ Current Type	Voltage	Charging Speed	Full Charge Time	Common Use / Location	Notes
L1 (AC)	120 V	Slowest	22–40 hours	Home (backup charging)	Included with most EVs and PHEVs; basic and low-cost option (evesco).
L2 (AC)	208–240 V (USA)230 V single-phase / 400 V three-phase (EU)	Up to 19× faster than L1	4–10 hours (typical)	Home, workplace, public stations	Requires dedicated charging unit; most common non-DC charging method (evesco).
L3 (DC Fast Charging)	400–900 V DC	Fastest	0.5–1 hour (to 80%)	Public fast-charging stations	High power (50–350 kW)



Figure 2.15- Overview of EV charging levels [30]



Figure 2.16- Common connectors for E-buses

2.4- Solar energy integration with EV Charging infrastructure

The integration of solar-based EV charging infrastructure is essential when discussing E-mobility. When the energy mix is not clean a BEV may produce higher life cycle CO_2 ($LCCO_2$) emissions compared to an ICEV. The example of China, where a significant share of electricity is still generated from coal, illustrates this clearly [38].

A typical charging infrastructure comprises a power system, an energy storage system, a communication network, and various charging ports and connectors, as illustrated in Figure 2.17. The power system provides a stable energy supply, increasingly supported by solar PV sources, either standalone or in combination with the grid. Battery energy storage systems (BESS) complement solar PV by storing excess energy and managing peak load demands, thereby ensuring uninterrupted service. The communication system enables real-time data exchange between chargers, vehicles, and management platforms, supporting functionalities such as user authentication, billing, load balancing, and remote diagnostics [39]. Charging ports and connectors vary globally, with standards such as CHAdeMO, CCS, and GB/T, ensuring compatibility across different vehicle types. Integrating solar PV into this system not only reduces reliance on fossil fuels but also supports a cleaner, more resilient mobility ecosystem [40].

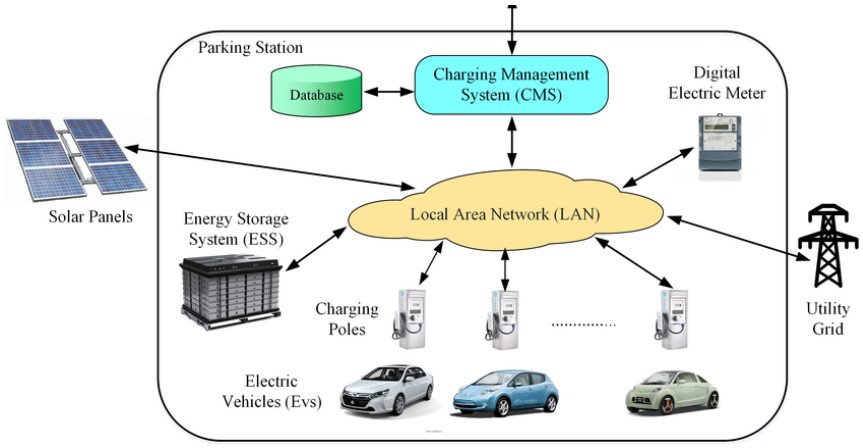


Figure 2.17- An overview of EV charging infrastructure [41]

2.4.1- Off-grid charging station configuration

Unlike on-grid systems, off-grid systems operate independently and are generally used in remote areas where the electricity grid does not reach or where connection fees for grid access are relatively high. Not being connected to the electrical grid, the DC produced by the PV array is stored in batteries and if necessary, it is also converted into AC energy through inverters. Figure 2.18 is a schematic illustration an autonomous charging station powered by a hybrid distributed energy resource. There are several possible configurations of an off-grid charging

station, depending on the location, weather conditions, and the local solar resource. The figure 2.18 below shows some of the possible configurations of an off-grid EV charging station.

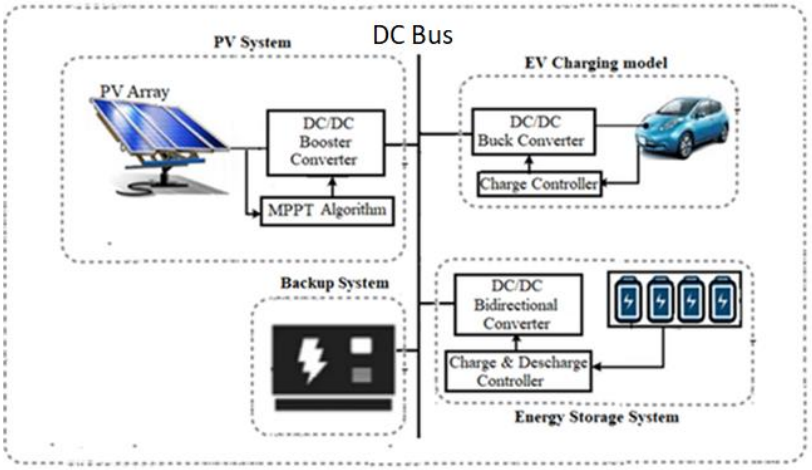


Figure 2.18- An Off-grid PV-based EV charging station diagram

2.4.2- On-grid Charging Station Configuration

On-grid EV charging stations are directly connected to the public electricity grid and represent the most adopted configuration, particularly in urban and peri-urban area. In this setup, PV energy is primarily utilised for self-consumption, while any surplus can be exported to the grid, if permitted by local regulations, or curtailed in zero-export systems. Conversely, during periods of low solar production, such as cloudy days or at night, the grid supplies the required energy to maintain uninterrupted charging operations. Figure 2.19 is a schematic illustration an on-grid charging station. As described by Twidell and Weir [42], inverters used in these systems synchronise the output of the PV array with the grid by tracking the grid voltage frequency, ensuring a smooth and compliant energy injection.

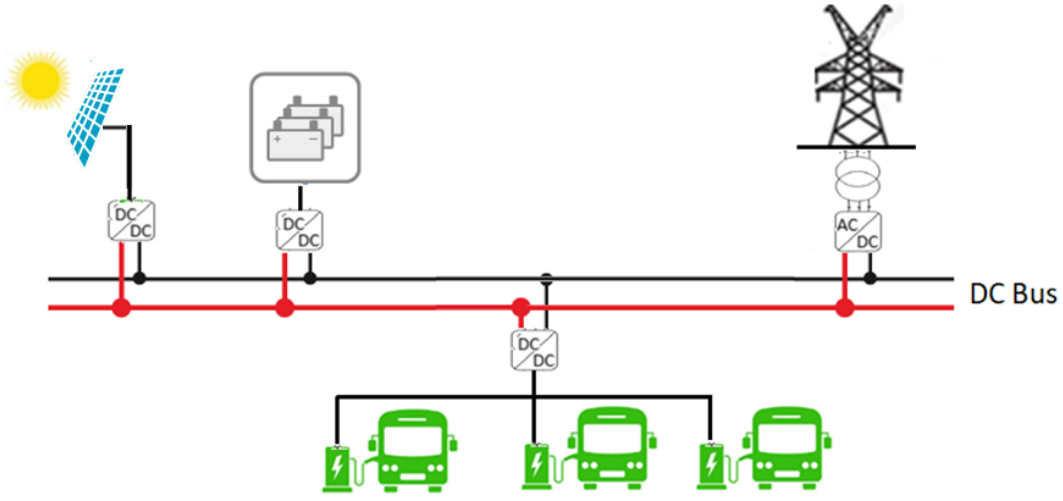


Figure 2.19- schematic illustration an on-grid charging station (Authors)

2.4.3- Zero-export systems

A zero-export system refers to a grid-connected PV installation designed to ensure that no excess solar energy is injected into the public electricity grid. This configuration is often implemented in areas where utility regulations restrict or prohibit energy export, or where grid infrastructure limitations require strict control over distributed generation. To ensure zero-export operation, systems typically incorporate Zero Export Devices (ZEDs), as illustrated in Figure 2.20, or smart inverters that continuously monitor both load demand and solar generation. The ZED functions as a protection and energy management system, continuously monitoring PV generation and grid consumption. It dynamically adjusts the PV system's output to match on-site demand, ensuring full compliance with zero-export regulations and preventing any excess energy from being fed into the grid [43] [44] [45].



Figure 2.20- Zero export device [45]

In the context of EV charging infrastructure, such as those for E-Buses, zero-export configurations allow solar energy to directly power charging stations while avoiding reverse power flow. This is particularly advantageous when paired with predictable charging schedules, such as mid-day layovers, aligning with peak solar generation. These systems improve self-consumption, reduce grid dependency, and avoid the need for feed-in tariffs or complex interconnection agreements.

However, without an energy storage system, surplus solar production must be curtailed during low-demand periods, leading to reduced solar utilisation. The integration of BESS helps address this issue by storing surplus energy for later use [46]. Figure 2.21 illustrates a typical configuration of a zero-export EV charging system, highlighting the integration of PV, ZED, BESS, and the charging station. Overall, the use of ZEDs enables compliance, grid protection, and optimised self-consumption in solar-powered charging applications.

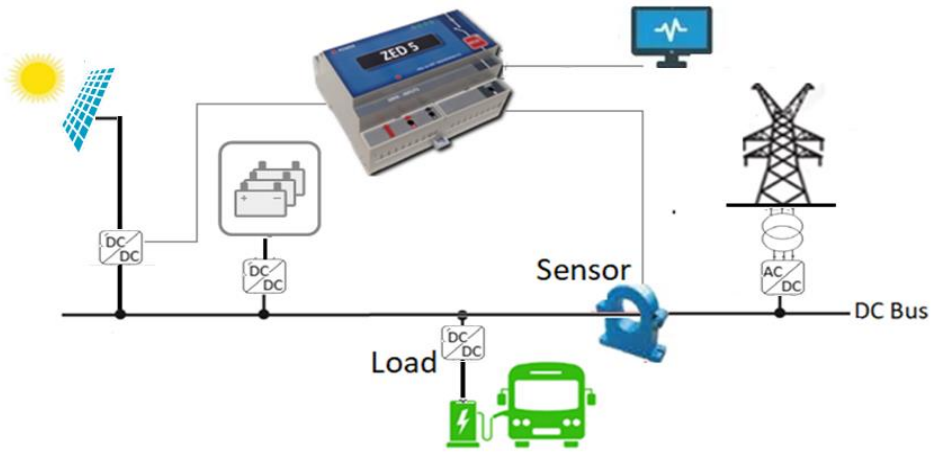


Figure 2.21- A typical configuration of a zero-export EV charging *system with a BESS*

2.5- State of the Art: Market Share, Challenges and Trends

This section presents a brief overview and state of the art of the technologies relevant to the topic of this dissertation. The chapter covers PV, EV and EV charging technologies.

2.5.1- PV Market Share, Challenges and Trends

The state of the art in PV technology is constantly evolving with ongoing research aimed at increasing efficiency, reducing costs and expanding the range of applications. Since the production of the first functional solar cell, made from silicon, with an efficiency close to 6%, by a group of researchers from Bell Laboratories, in 1954, we are in the fourth generation of PV cells, as the flowchart in Figure 2.20 illustrates. However, due to their relatively high market share and efficiency, as shown in Figure 2.22, silicon devices dominate the current market[47].

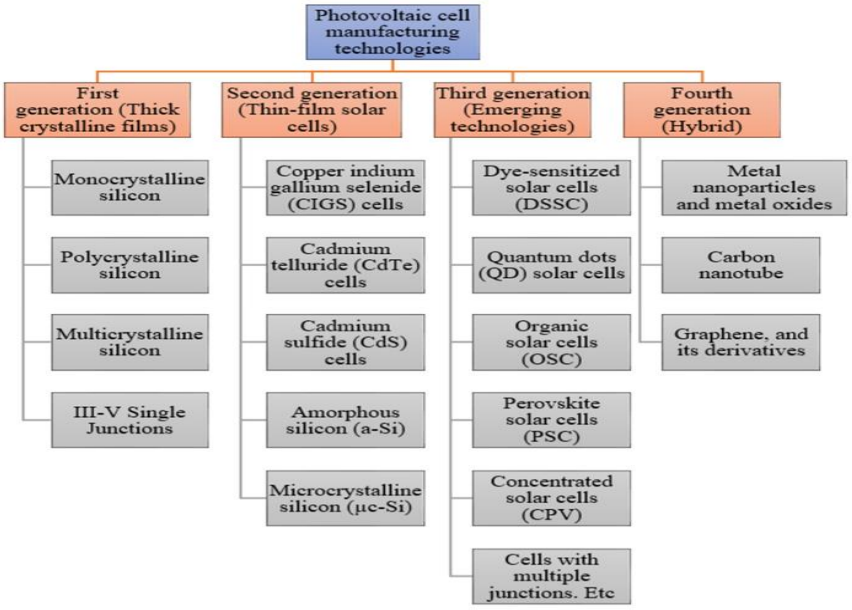


Figure 2.22- PV cells generations and their current developments [31]

1st generation: This generation include crystalline silicon (c-Si) solar cells, which dominate the market due to their relatively high market share and efficiency. However, this generation of PV cells still has high production costs, their manufacturing processes are extremely complex, and in addition they have higher temperature sensitivity [47].

2nd Generation: This generation emerges in order to counteract the disadvantages inherent to silicon cells. It includes thin-film solar cells with advantages like flexibility, lower manufacturing costs, and potential for advanced applications. However, in addition to the toxicity of materials used in this generation of PV cells, such as cadmium (Cd) and selenium (Se) found in Cadmium Telluride (CdTe), Copper Indium Gallium Selenide (CIGS), and Copper Indium Selenide (CIS) PV cells, the availability of these materials is limited.

3rd Generation: Among other factors, this generation emerges due to the high cost of first-generation cells, limited availability and toxicity of materials for second-generation cells. Furthermore, this generation emerges to surpass the Shockley-Queisser efficiency limit.

4th Generation: This generation include technologies like quantum dots, nanowire solar cells, and multi-junction solar cells. This generation focus on further improving efficiency, durability, and scalability, combining the low cost and flexibility of polymer thin films, with the stability of organic nanostructures. However, the technologies used for third and fourth generation cells are still in the prototyping stage [47].

a) Market share of PV panels

Due to the abundance and availability of the silicon, which is therefore relatively cheap, around 95 % the total market share of solar cells comes from crystalline silicon material [48]. Due to low efficiency ratios, amorphous silicon (a-Si) products have been discontinued in recent years, resulting in a negligible market share today. Figure 2.23 illustrates the projected market share of PV Technologies during the forecast period from 2024 to 2030 [49].

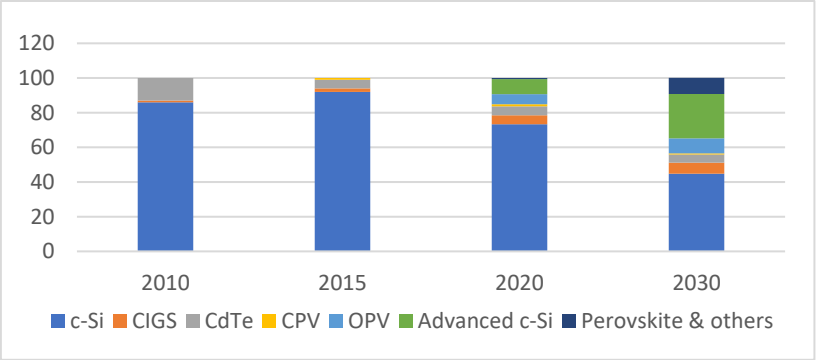


Figure 2.23- Global PV Market Share by Technology, 2010-2030 [33]

2.5.2- EV Market Share, Challenges and Trends

The current state of the art in urban mobility remains dominated by ICEVs. Nevertheless, EV adoption is growing rapidly, driven by policy incentives, falling battery costs, stricter emissions regulations, and technological advancements in electric drivetrains and charging infrastructure. This shift aligns with global efforts to reduce Greenhouse gases (GHG) emissions and improve energy efficiency within the transport sector [38], [50], [51].

Modern EVs now offer competitive performance, with extended driving ranges, fast-charging capabilities, and lower operational costs when compared to ICE counterpart. Innovations such as solid-state batteries, vehicle-to-grid (V2G) integration, and AI-assisted energy management systems are redefining the possibilities of electromobility. Barbosa [52] emphasizes that these developments, largely shaped by cross-sectoral innovation, have paved the way for the large-scale deployment of electromobility across light-duty and heavy-duty segments.

In the transit sector, Battery Electric Buses (BEBs) represent a key technological frontier. Unlike traditional trolleybuses that rely on fixed overhead power networks, BEBs offer greater operational flexibility and can be deployed in low- to medium-demand corridors thanks to improvements in battery reliability and durability [52], [53]. The Figure 2.24 below shows modern urban E-buses in operation in some urban areas in Europe.



Figure 2.24- Articulated urban buses: (a) Hybrid- Rome, (b) Full-electric- Berlin, 2025 (Author).

a) Market share

As of 2019, approximately 18% of the global bus fleet operated using electric power sources. This figure includes battery electric buses (6.3%), hybrid-electric models (7.9%), and those powered by direct overhead wires or similar technologies [7]. The momentum continued into 2020, with the global stock of electric passenger cars growing by about 40%, and more than 600,000 electric buses deployed worldwide.

Forecasts for the period from 2024 to 2030 indicate that the global market for electric bus, predominantly city buses will grow from USD 17.0 billion to USD 37.5 billion, representing a compound annual growth rate (CAGR) of approximately 14.2% [54]. The Asia-Pacific region is anticipated to remain the dominant market, driven by leading manufacturers such as BYD and Yutong, which offer a wide range of competitively priced E-Buses across major global markets. This trend is illustrated in Figure 2.25.

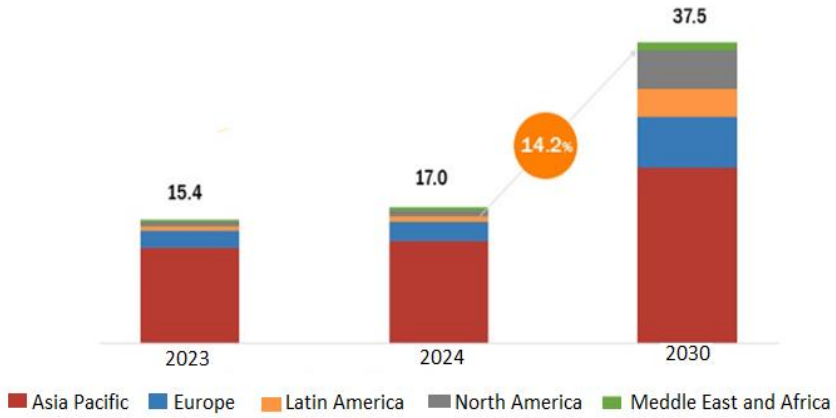


Figure 2.25- Electric bus market share by region, 2024-2030 [34]

b) Challenges in Adoption

Despite the accelerating global transition, several barriers hinder widespread EVs and E-Buses deployment, particularly from the perspective of public transit agencies. As an innovative technology, the high acquisition cost of EVs coupled with the limited availability of charging infrastructure, represents one of the primary challenges to the widespread adoption of E-buses [37], [54], [55].

Another challenge, when it comes to the E-bus adoption is the adverse effect of uncontrolled charging on the electricity grid, given the high power needed for recharging E-bus fleets [37], [54]. According to the conclusions of Ashkezari1, Kaleybar And Brenna [37], the solution to this problem involves the addition of stationary ESS or energy production near charging stations, as well as the integration of renewable energy sources (RES) into the grid.

As Sclar, Gorguinpour, Castellanos, and Xiangyi Li [56] outline, these barriers can be subdivided into technological, financial, and institutional challenges within vehicles and batteries, agencies and operators, and grid and charging infrastructure dimensions.

Technological Barriers: Persistent issues include limited range, battery degradation, and performance variations under extreme temperatures. For e-buses, range limitations remain one of the most consistent challenges across all stages of adoption[56], [57].

Financial Barriers: High upfront costs of e-buses and charging infrastructure continue to constrain adoption, particularly for cash-strapped transit agencies. Although lifecycle costs are often lower due to reduced maintenance and fuel expenses, securing initial capital investments remains a major obstacle [56], [57]

Institutional Barriers: Limited technical expertise, lack of standardized data, and fragmented policy frameworks impede project implementation. Agencies often struggle with integrating e-bus operations into existing transit systems and coordinating among multiple stakeholders, from utilities to municipal planners [56].

c) Trends and Outlook

Looking forward, several key trends are shaping the evolution of EV technology and markets:

Battery Innovation and Cost Decline: Continued improvements in battery chemistry and manufacturing will reduce costs and enhance vehicle performance, making EVs increasingly competitive.

Decentralized Charging Infrastructure: Growth in ultra-fast chargers and wireless charging technologies will enhance convenience and operational efficiency, particularly for urban transit and logistics fleets.

Grid Integration and Renewable Energy Synergies: The convergence of EV deployment with renewable electricity generation and energy storage solutions will enhance the environmental benefits of electrified mobility [52], [58].

By 2030, electric mobility is projected to become a mainstream transport solution, representing a transformative shift toward cleaner, more efficient transportation systems. However, realizing this potential will depend on overcoming the technical, financial, and institutional barriers that persist across markets and vehicle categories.

2.5.3- E-Bus Charging Market Size, Challenges and Trends

Advancements in PV technology have significantly influenced the development of EV charging infrastructure, particularly within public transportation systems. Solar-powered EV charging stations are emerging as a viable solution to support the increasing global demand for

clean and sustainable mobility. These systems utilize energy from solar panels to charge electric buses, contributing to the decarbonization of urban transport.

One example is the solar-powered charging system implemented by Transdev in Brisbane, Australia. The system includes a 135 kW ESS supported by 250 solar panels, which generate an average of 438 kWh per day. This energy is used to charge Transdev's E-Buses equipped with a 348kWh battery capable of delivering up to 300 km per charge under at NOCT conditions, as illustrated in Figure 2.26 [59]. Similarly, large-scale networks such as ChargePoint, with over 30,000 charging ports across North America, reflect the growing presence of solar-integrated EV charging infrastructure [60]. Another example is the Brookville Smart Energy Bus Depot in Maryland, USA, which powers 70 electric school buses with a 4.14 MW solar microgrid. Supported by a 3 MW/4.3 MWh battery system, the depot ensures resilience during outages and supports grid stability through demand response [61]. This integrated approach to E-bus charging is illustrated in Figure 2.26



Figure 2.26- An integrated system for E-Bus charging at Transdev's Capalaba Depot [36]

a) Market share

The global E-Bus charging station market has experienced substantial growth and is projected to expand significantly between 2026 and 2033. The prevailing upward trend in market dynamics and anticipated expansion signal robust growth rates throughout the forecasted period. In essence, the market is poised for remarkable development. According to Verified Market Reports [62], major players in this sector include ABB, Siemens, Blink Charging, ChargePoint, Schneider Electric, Tesla, Proterra, BYD, Ionity, Electrify America, Trucking

and Bus Corporations. Figure 2.27 illustrate the global E-Bus charging station market size and scope.

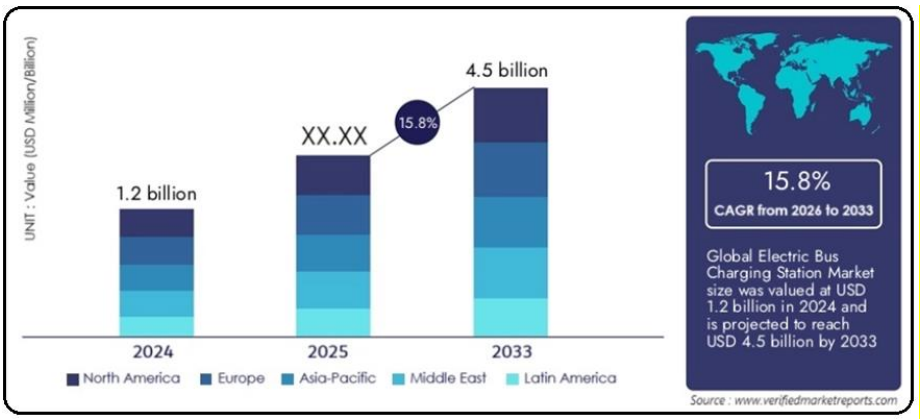


Figure 2.27- Global E-Bus charging station market size and scope by region, 2024-2033 [62]

b) Challenges and trends

The integration of E-bus charging infrastructures brings about both positive and negative impacts on the electrical grid, as summarized in the Figure 2.28. PV-based charging systems provide environmental and operational benefits, however, their integration into existing electrical grids also presents challenges. These include grid load fluctuations, infrastructure costs, and the need for intelligent energy management systems to coordinate charging schedules with solar availability. Nonetheless, new trends are emerging to address these issues. The use of smart inverters, energy storage systems, and grid-friendly technologies like Vehicle-to-Grid (V2G) and demand-side management are improving grid compatibility and efficiency.

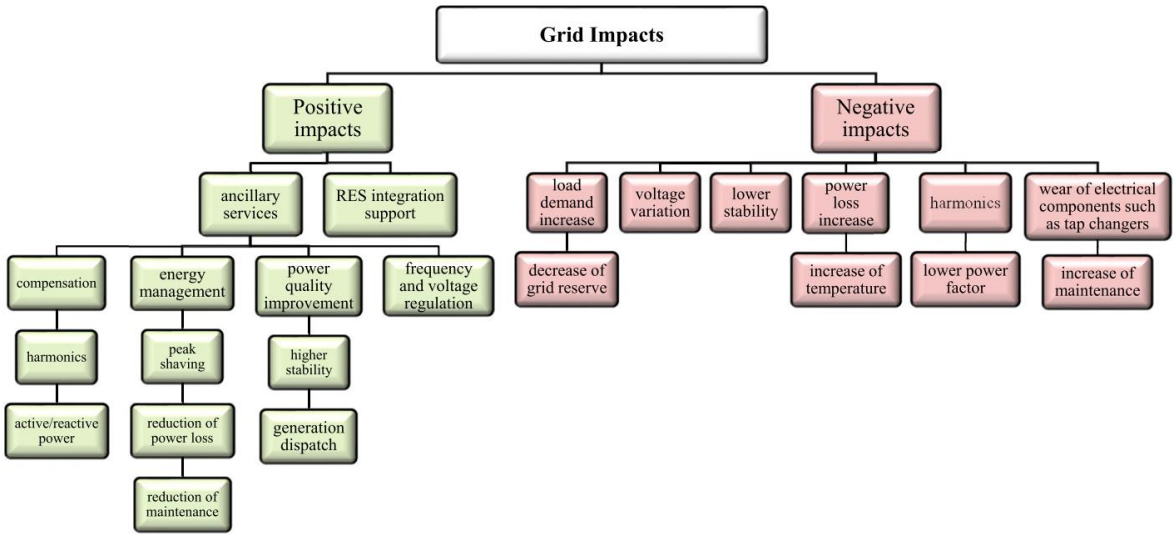


Figure 2.28- Impact of E-Bus charges on the grid [29]

Chapter 3 : MATERIALS AND METHODS

This chapter provides a detailed description of the materials and methods used to design, model and evaluate a grid connected PV-based charging infrastructure for E-buses. The system operates under strict self-consumption conditions, ensuring that no energy is exported to the grid. Instead, the grid serves as a backup source, supplying electricity only when the PV generation cannot meet the demand. The methodological approach is structured into three stages:

- Modelling the e-bus load profile: Based on vehicle, road and operational parameters;
- Assessing the local solar PV potential: Based on the PVGIS-SARAH2 database and;
- Sizing the grid-connected PV-based charging station: Based on e-bus load profile and local solar PV potential.

3.1- Case Study Description

The study focuses on the BRT N1 line as per the Comprehensive Urban Transport Master Plan for the Greater Maputo. The charging station is designed based on the estimated daily and annual energy demand of articulated electric buses, considering the vehicle, route and operational parameter. The route comprises a 19.1 km extension, from Maputo Terminal (Mpt) to Zimpeto Terminal (Zmpt), which is 38.2 km round-trip. In the same route, there are three proposed terminals, as shown on the map in the Figure 3.1. Figure 3.2 shows the overall layout of Mpt and Zmpt respectively.



Figure 3.1- Map of the BRT N1 line [15]



Figure 3.2- Overall layout of (a) Maputo and (b) Zimpeto Terminals & Depots [15]

3.2- Electric Buses load Profile

At a strategic level, energy consumption estimation models for EV can among other things, be used to define the installation of charging infrastructure and fleet sizing [63]. In this study, the E-Bus energy demand is modelled by using a physics-based approach, consisting of modelling the longitudinal dynamics of the vehicle.

3.2.1- Physical Model

Among others, the physical models can potentially yield the most accurate results [64]. Up to date, a variety of different physical models with different grades of detail have been proposed. When it comes to the power consumed for vehicle motion, the most common approach as, is the longitudinal model, which consist of modelling the longitudinal dynamics of the vehicle, by applying Newton's second law. The graphical representation of the forces acting on the vehicle is provided in Figure 3.3. By modelling each of these forces, the electric power demanded by the powertrain (in kW), in each segment of the route can be calculated as Equation (3.1) [65].

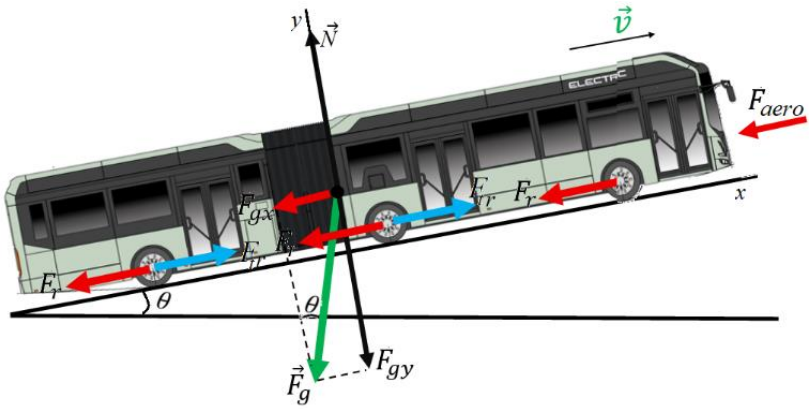


Figure 3.3- A schematic view of the longitudinal forces acting on the vehicle

$$P_{DC}(t) = \frac{1}{1000\eta}\left\{Mg[sin\theta + C_r cos\theta] + \frac{1}{2}\rho C_d A_f v(t)^2 + \delta Ma\right\} v(t) \quad (3.1)$$

The EV energy model parameters considered, include total mass (M), operating speed (v), rolling resistance coefficient (C_r), aerodynamic drag coefficient (C_d), frontal area (A_f), air density (ρ) and road gradient (θ), and factors such as the overall powertrain efficiency (η) and the inertia factor of all rotating components δ [66]. Powertrain efficiency varies with driving conditions, and is calculated differently as Equation (3.2) depending on whether the tractive force is positive (energy demand) or negative (energy regeneration) [67].

$$\eta = \begin{cases} \frac{1}{\eta_{reg}\eta_{TG}\,\eta_i\,\eta_m}, & F_{tr}(t) < 0 \\ \eta_{TG}\,\eta_i\,\eta_m & F_{tr}(t) \geq 0 \end{cases} \quad (3.2)$$

Where η_{TG} is the efficiency of the transmission and gearbox, η_i is the efficiency of the inverter, η_m is the efficiency of the motor, and η_{reg} is the regeneration factor. As the bus route is fixed and the trip distance is known, the total energy consumption E_L for a trip can be calculated as Equation (3.3). The auxiliary power (P_{aux}) covering systems such as steering, doors, lighting, displays and air condition, needs to be taken into account [68], [69], [70]. In this study, P_{aux} is assumed to be constant and to represent 20% of the total powertrain demand.

$$E_L = \int_{t_0}^{t} (P_{DC}(t) + P_{aux})\, dt \quad = \quad 1.2 \int_{t_0}^{t} P_{DC}(t)\, dt \quad (3.3)$$

3.2.2- Physical Model Input parameters

The daily operation of the E-bus fleet was modelled based on the predominant mobility flows in the Maputo Metropolitan Area, with inbound during morning peak hours and outbound in the afternoon. To accurately match the energy demand without overestimating consumption, a fleet of three E-buses was considered. Each bus performs two inbound trips in the morning and two outbound trips in the afternoon. This results in a total of four roundtrips or, when optimized, can be arranged as three complete round trips per day. A round trip comprises two consecutive trips in opposite directions (Zmpt to Mpt and return). Due to variations in road gradient, the energy consumption differs between outbound and inbound journeys. Therefore, the energy demand of each round trip is calculated by summing the specific energy consumption of both directions. Each trip is composed of a sequence of driving cycles, which represent bus movement between consecutive stations and include acceleration, cruising, deceleration, and stop time. The duration of each trip is calculated from the 19.1 km route

distance, with an additional 20% to account for delays at traffic signals [71], as well as a scheduled layover of 30 minutes at each terminus.

Bus departures are scheduled at 30-minute intervals from 06:00, with midday layover after completing the morning operations, resuming at 15:00 for the afternoon peak, before resting overnight. Charging is carried out during all resting periods, ensuring adequate energy availability for subsequent operations. Figure 3.4 illustrates a representative driving cycle, while Figure 3.5 depicts the daily operation cycle.

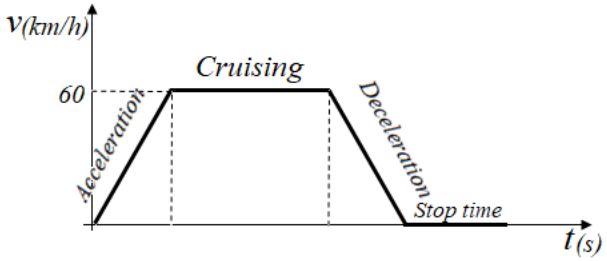


Figure 3.4- Bus driving cycle diagram (author)

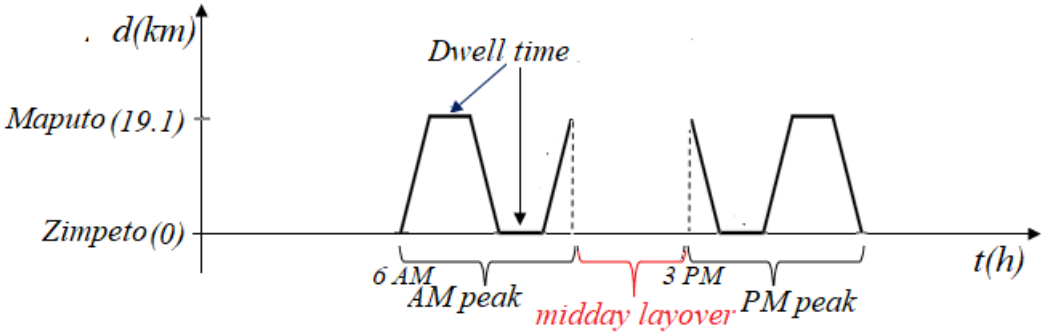


Figure 3.5- Daily bus operation cycle diagram (author)

3.2.3- Physical Model Input parameters

In order to estimate energy demand, it is necessary to define the vehicle, route and operational parameter. The vehicle-related parameters include all the powertrain components. The operational parameters are related to how the vehicle operates on the road, taking into account not only the predefined rules, but also the behaviour of the driver when accelerating or decelerating, which leads to an increase in the total energy consumption [65]. The procedures and sources adopted for data acquisition in this study are described below, and all parameters are summarized in the Annex C.

a) Vehicle Parameters

The vehicle parameters were obtained directly from the official technical datasheet of the manufacturer, with the 18 m Volvo 7900 articulated E-bus as the reference model, as shown in **Annex A**. Other physical parameters not explicitly provided by the manufacturer were

estimated based on values reported in the technical literature. In this study, the mass of the vehicle (M), provided by the vehicle manufacturer [72] is calculated as the gross vehicle weight rating (GVW), which is the maximum allowable mass of a road vehicle or trailer when loaded, including the weight of the vehicle itself plus fuel, passengers, cargo, and trailer weight.

c) Operational Parameters

The operational parameters define the conditions under which the vehicles operate along the fixed route. These parameters are essential to simulate the vehicle's energy consumption along its route. In this study, the main operational parameters such as the operating speed of 60 km/h, dwell time of 20 seconds, and layover of 30 minutes at terminus, were extracted from the proposed BRT system, as documented in the reports of the Comprehensive Urban Transport Master Plan for Greater Maputo [16]. According to the BRT standard, for pedestrian convenience and BRT operational efficiency, the recommended distance between stations should be on average between 0.3 km and 0.8 km [73]. However, for calculation simplicity, a segment length of 1.0 km is adopted in this study.

d) Route Parameters

Route parameters refer to the fixed physical features and geographic layout of the corridor, independent of driving behaviour or operational strategies. These include total route length, number of stops, average stop spacing and elevation. These latest data were extracted from the proposed BRT system and confirmed using OpenStreetMap Automated Navigation Direction (OsmAnd).

The elevation data were extracted from high-resolution digital terrain models. To incorporate the route's topography into the Physical model, the elevation profile was extracted via OsmAnd, a GPS software based on OpenStreetMap data. The model was discretized for each 1.0 km driving cycle, with three phases (acceleration-cruise-deceleration) segment. The entire route was first divided into segments based on significant changes in elevation, by identifying local maximum and minimum points. The road slope as illustrated in Figure 3.6 is calculated using Equation (3.4), where Δh denotes the elevation change and Δx refers to the horizontal distance.

$$\text{slope}\% = \frac{\Delta h}{\Delta x} \times 100 \tag{3.4}$$



Figure 3.6- The proposed BRT N1 road gradient map [74]

3.3- Solar Resource Profile

The data ware obtained from the PVGIS-SARAH2 platform, a geostationary METEOSAT satellite-based database, covering Africa, Europe and Asia, as shown in Fig 3.5. The data under consideration represent a Typical Meteorological Year (TMY), with hourly resolution for the reference period 2005-2020. The TMY, originally created by Sandia National Laboratory is a set of 12 months chosen as the most typical and representative out of the full time period available. The input files include the following datasets:

- Hourly Global Horizontal Irradiance (GHI);
- Optimal Monthly Global Tilted Irradiance (GTI);
- Hourly Wind speed at 10 meters above the ground (w);
- Hourly average temperature at 2 m above the ground (T_a).

After collecting the above-mentioned data, a statistical method was applied to perform temporal aggregation, resulting in monthly daily averages and annual daily average tables, using Microsoft Office Excel. The results were then compared with SOLARGIS solar resource maps and findings from previous studies.

Using the GHI and GTI at the optimum tilt angle data, a histogram of monthly average daily irradiance was generated. To represent the seasonal behaviour of the system, four typical days corresponding to the equinoxes and solstices were selected. Based on hourly GHI data, seasonal typical day curves were plotted to illustrate the daily variation in irradiance.

Subsequently, under STC, the P_{DC} of the module was determined using Equation (3.5), taking into account optical and thermal losses. The operating temperature of the PV module was

determined using the Duffie-Beckman model Equation (3.6) [21]. As the mounting configuration strongly influences the NOCT [75], the INOCT condition was considered within this model. The simulations is based on the c-Si PV cell technology, as shown in the Table 3.1, as specified in the annexe B.

Table 3.1- PV module specifications

PV Model	Nominal Power (W)	Nominal efficiency
SPR-X21-460-OM	460	21.3%

$$P_{DC} = P_{STC}\left(\frac{G_M}{G_{MSTC}}\right)[1 + \alpha(T_C - T_{STC})] \quad (3.5)$$

$$T_C = T_a + \left(T_{C,INOCT} - 20\right)\frac{G_M}{800} \cdot \frac{9.5}{5.7+3.8w}(1 - 0{,}9) \quad (3.6)$$

3.3.1 PVGIS-5.2 Spatial and Temporal Coverage and resolution

PVGIS is a free access web application that provide solar and climate data and PV systems performance assessment tools for any place in most parts of the world according to the coverage achieved by the satellites, as shown in Figure 3.7. In the case of the PVGIS version 5.2 used in this study, the spatial coverage is ±65° longitude and ±65° latitude, and the time coverage is from 2005 to 2020.

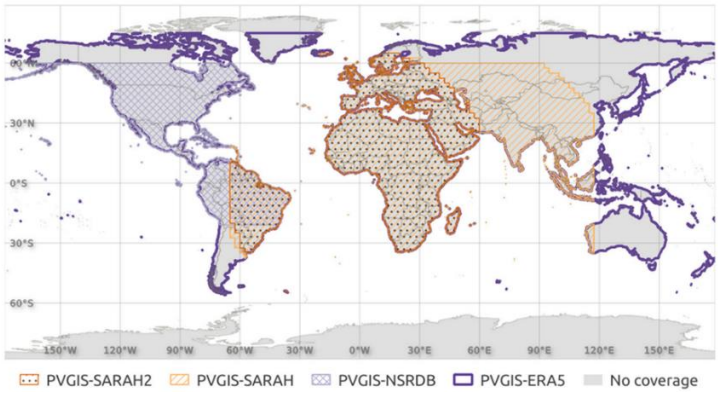


Figure 3.7- PVGIS-5.2 Spatial coverage [50]

Table 3.2- PVGIS-5.2 Spatial and Temporal Resolution

	Spatial resolution	**Temporal resolution**
Solar radiation	5 x 5 km	1 h
Temperature	9 x 9 km	1 h
Wind speed	9x 9 km	1h

3.4- PV charging station Design and Sizing

3.4.1- Charging System Configuration and Operation Mode

In this study, the charging station is designed to operate in grid-connected with zero-export mode, prioritizing SC as illustrated in Figure 12. Zero-export operation consists of fully preventing any injection of surplus energy into the utility grid, and it has been adopted for several years in various countries for specific applications**.** In this configuration:

- No energy is injected into the grid;
- PV generation supplies the E-Bus directly;
- Surplus PV energy charges the BESS;
- The BESS discharges during peak demand or low solar availability;
- The grid supplies power only when both PV and BESS are insufficient to meet the load.

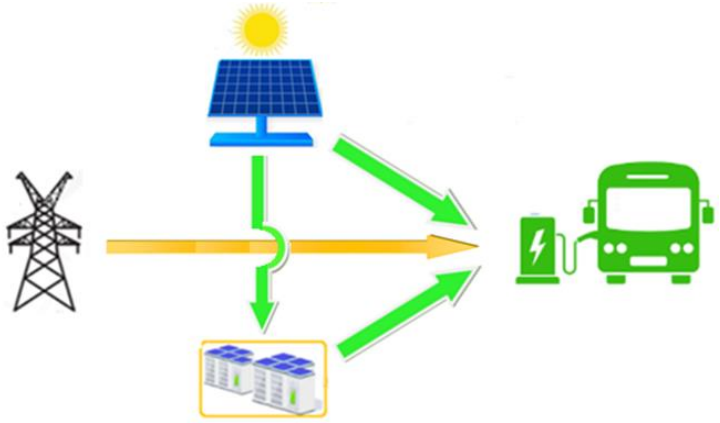


Figure 3.8- An innovative energy system power flow

3.4.2- Charger Sizing for Midday Energy Demand

The charger capacity should be sized to fully supply the buses' daily energy demand during the midday PSH. By matching the charging power to the energy required within the limited solar generation window, the system maximizes renewable energy use and ensures buses are fully charged for daily operations. Mathematically, the required charger power can be estimated as Equation (3.7):

$$P_{Charger} = \frac{E_{daily}}{PSH} \tag{3.7}$$

where E_{daily} is the bus or bus fleet's total daily energy demand, and PSH is the duration of peak solar irradiation. In this study, the CCS2 charger was selected for simulation, as it is the recommended standard for the e-bus model considered, as specified in Table 3.3 and detailed in Annexes A and B, respectively.

Table 3.3-EV Charger specification

EV Charger Model	Output Power rating (kW)	Nominal Efficiency
CCS2	50	>93%

3.4.3- PV System Sizing

There are many different ways of designing PV systems, in this study, assuming self-consumption as a viable option for distributed generation, the system design is based on the Manual de Engenharia para Sistemas Fotovoltaicos from CEPEL-CRESESB [28] and reference [75].

a) Installed PV Capacity Calculation

The calculation of the peak power P (kW_P), which is important for sizing the photovoltaic array, is given by the value of the energy that the PV system should produce daily, divided by the PSH as Equation (3.7). As explained in the section 2.4, PSH corresponds to the number of hours during which solar radiation is constant and has a value of 1 kW/ m^2 at a given location.

$$P_{STC} = \frac{E_L}{PSH \times PR} \tag{3.7}$$

Where E_L is the energy demand (kWh) and PR is the performance ratio (dimensionless), given as $Red_1 \times Red_2$. Red_1 is the power derating factor due soiling, physical degradation, losses due temperature shedding. For c-Si PV modules, this factor is assigned a default value of 0.75. Red_2 is the power derating factor due cabling, controller diodes, etc, and a default value of 0.9 is recommended for this factor.

b) Calculating the number of modules (N)

$$N = 1000 \times \frac{P_{STC}}{P_m} \tag{3.8}$$

P_m is the nominal power of the module.

c) Rough area estimate

$$A_r = N \times A_m \tag{3.9}$$

To estimate the total area needed for a PV installation, two commonly used preliminary methods are spacing factor, commonly 10–30% to account for maintenance walkways, mounting structures and small gape, and Ground Coverage Ratio (GCR). Typical GCR values for rooftop PV range from 0.6 to 0.9, depending on tilt, latitude, and spacing needed to avoid inter-row shading and allow access.

Applying a spacing factor of 30% to account for maintenance walkways, mounting structures and small gapes the total area will be estimated as Equation (3.10).

$$A_t = A_r \times 1.3 \tag{3.10}$$

Using GCR for full shading space of 0.60, the total area will be estimated as Equation (3.11)

$$A_t \ \frac{A_r}{GCR} = \frac{A_r}{0.60} \tag{3.11}$$

These methods provide only a preliminary estimation of the required area. The actual PV layout should be determined based on the available roof or site area, taking into account the exact roof dimensions and shape, orientation and tilt constraints, obstacles (chimneys, vents, equipment), shading from nearby structures or trees, etc. Once the site-specific conditions are known, a detailed layout study should be performed to refine the total area, number of modules, and spacing.

After obtaining the size of the PV System from the formula-based process, it is recommended that the system be optimised. The optimization process can be carried out either using computer tools (Homer Grid, PVSyst, SAM, iHOGA, PVGIS, etc) or by manually. However, in this study, PVGIS was used, as it is a free-access web application that, in addition to providing solar and climate data, also serves as a PV System performance assessment tool.

Chapter 4 : RESULTS AND DISCUSSIONS

4.1- E-bus Energy Demand profile

The e-bus energy profile is based on driving cycles simulation along the route. This simulation reflects the typical motion of a bus operating in an urban BRT corridor. The spatiotemporal profile of the vehicle's velocity features the three distinct phases, as illustrated in Figure 4.1. The analysed driving pattern suggests a significant energy consumption during the acceleration phases until cruising speed is reached, as well as energy losses during deceleration phases, considering that regenerative braking is not fully efficient.

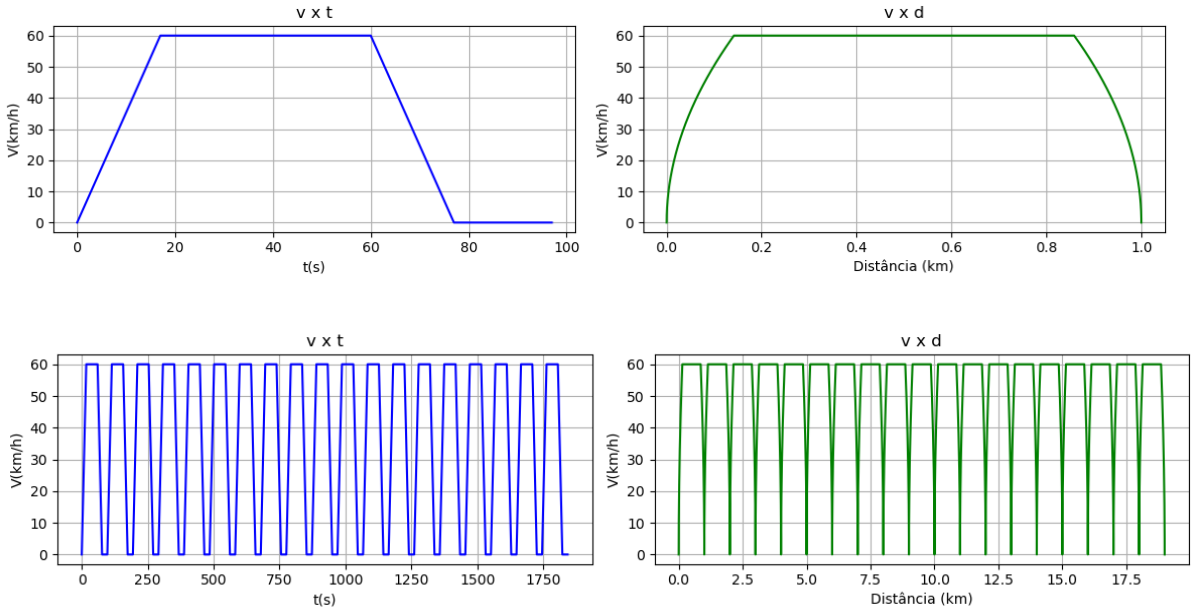


Figure 4.1- Simulated driving cycles in spatiotemporal domains: (a, b) 19 cycles; (c, d) one cycle

4.1.1- E-buses Specific Energy demand

The energy consumption is calculated considering elevation difference between the Zmpt and Mpt, as depicted in Figure 4.2. Through OSM, it was found that the total elevation gain is 21m (decent on the inbound and acescent on the outbound tip). In this case, there is a slope of 0.11% corresponding to 0.063^0.

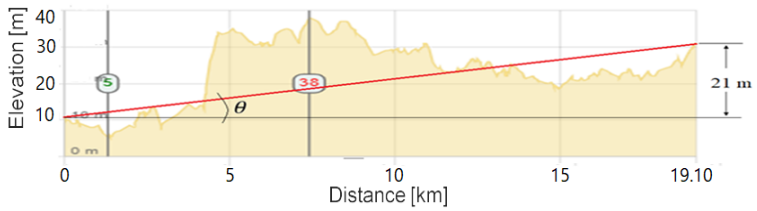


Figure 4.2- Route altimetry according elevation difference between the two terminals

Based on the physical model, accounting for the overall powertrain efficiency, the specific electrical energy consumption for road gradients between 0.11% and 0.55% ranges from 1.30 to 2.52 kWh/km, with an average value of 1.91 kWh/km, as shown in Table 4.1. These results demonstrate the substantial impact of road gradient on energy demand, highlighting how variations in slope directly influence specific energy consumption throughout the route. It is important to note that this study does not account for energy losses during cornering, which may result in a slight underestimation of the actual energy consumption. Nonetheless, considering that In BRT systems, vehicles operate on dedicated lanes without constraints such as traffic congestion and irregular stops, which would reduce operational vehicle efficiency, the results are consistent with empirical observations and previous studies on 18 m articulate urban e-buses. These studies typically report specific energy consumption values ranging from 1.6 to 3.4 kWh/km, [67], [68], [76], [77], [78].

Table 4.1- Energy Performance overview per trip, for a slope of 0.11% and 0.55%

```
--- Energy Performance Overview per Trip (grad 0.11%) ---
                  section  Total Energy(kWh)  specific consumption (kWh/km)
outbound-trip (19 cycles)          33.976330                       1.788228
  return-trip (19 cycles)          38.637303                       2.033542
                    Total          72.613634                       1.910885

--- Energy Performance Overview per Trip (grad 0.55%) ---
                  section  Total Energy(kWh)  specific consumption (kWh/km)
outbound-trip (19 cycles)          24.654133                       1.297586
  return-trip (19 cycles)          47.958885                       2.524152
                    Total          72.613019                       1.910869
```

4.1.2- E-Buses Daily and Annual Energy Demand

Another important metric is the daily energy consumption. However, this metric will depend on the operational polices adopted by the operator. Based on the urban mobility pattern observed in the city of Maputo, as described in Section 3.2.2, two inbound and two outbound trips were organized in a way that results in three round trips. These were considered as the scope of this study and distributed throughout peak hours. The Table 4.2 indicates the daily E-buses operation pattern, and the Figure 4.3 shows the daily operational schedule.

Table 4.2- Daily Bus operation schedule

	Bus	From	To	Departure	Arrival
0	Bus 1	Zimpeto	Maputo	06:00:00	06:37:03
1	Bus 1	Maputo	Zimpeto	07:07:03	07:44:06
2	Bus 1	Zimpeto	Maputo	08:14:06	08:51:09
3	Bus 1	Maputo	Zimpeto	15:00:00	15:37:03
4	Bus 1	Zimpeto	Maputo	16:07:03	16:44:06
5	Bus 1	Maputo	Zimpeto	17:14:06	17:51:09
6	Bus 2	Zimpeto	Maputo	06:30:00	07:07:03
7	Bus 2	Maputo	Zimpeto	07:37:03	08:14:06
8	Bus 2	Zimpeto	Maputo	08:44:06	09:21:09
9	Bus 2	Maputo	Zimpeto	15:30:00	16:07:03
10	Bus 2	Zimpeto	Maputo	16:37:03	17:14:06
11	Bus 2	Maputo	Zimpeto	17:44:06	18:21:09
12	Bus 3	Zimpeto	Maputo	07:00:00	07:37:03
13	Bus 3	Maputo	Zimpeto	08:07:03	08:44:06
14	Bus 3	Zimpeto	Maputo	09:14:06	09:51:09
15	Bus 3	Maputo	Zimpeto	16:00:00	16:37:03
16	Bus 3	Zimpeto	Maputo	17:07:03	17:44:06
17	Bus 3	Maputo	Zimpeto	18:14:06	18:51:09

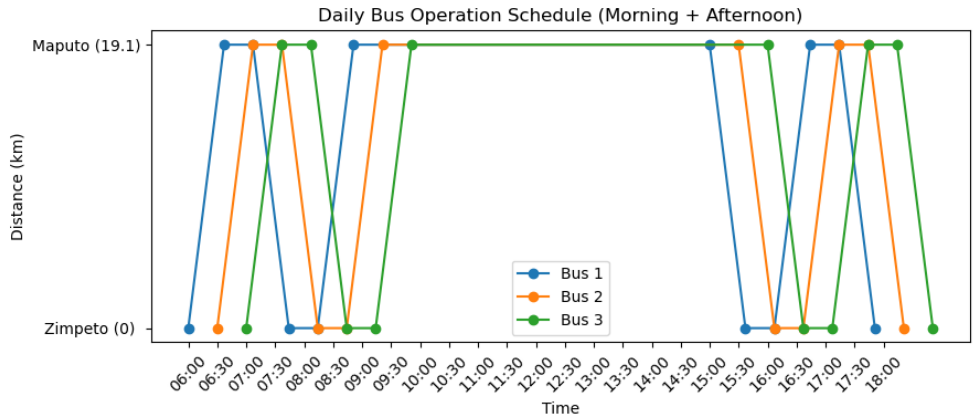


Figure 4.3- Daily E-bus operation pattern

From this perspective, considering 1.91 kWh/km as the approximate average of the e-bus specific energy consumption, a bus round-trip would require approximately 72,96 kWh at the powertrain level. When battery efficiency is taken into account, assuming a round-trip efficiency of 93%, the effective battery discharge energy increases to approximately 78.45 kWh per bus per round-trip. Considering an additional charging efficiency of 93%, the energy that must be supplied by the PV system reaches about 84.36 kWh per bus per roun-trip, as summarized in the Table 4.3.

As the case study considers three articulated electric buses operating under the same duty cycle, with each vehicle completing three cycles per day, covering a total distance of 114.6 km per day, the total daily PV energy required is therefore approximately 759.23 kWh, corresponding to about 277.12 MWh annually, which defines the minimum daily and annual energy generation needed for the PV-based charging infrastructure, respectively. All annual values for a fleet of three buses are summarized in the Table 4.4.

Table 4.3- Estimated daily and annual energy demand per E-bus

Cycles	Distance (km)		Energy demand (kWh)					
	Daily	Annual	Daily			Annual		
			$\eta_{Powertrain}$	$\eta_{Battery}$	$\eta_{Charger}$	$\eta_{Powertrain}$	$\eta_{Battery}$	$\eta_{Charger}$
1	38,2	13943,0	72,96	78,45	84,36	26631,13	28635,62	30790,99
2	76,4	27886,0	145,92	156,91	168,72	53262,26	57271,25	61581,99
3	114,6	41829,0	218,89	**235,36**	253,08	79893,39	85906,87	92372,98
4	152,8	55772,0	291,85	313,82	337,44	106524,52	114542,49	123163,97
5	191	69715,0	364,81	392,27	421,79	133155,65	143178,12	153954,97
6	229,2	83658,0	437,77	470,72	506,15	159786,78	171813,74	184745,96
7	267,4	97601,0	510,73	549,18	590,51	186417,91	200449,37	215536,95

Table 4.4- Estimated daily and annual energy demand for three E-bus fleet

Cycles	Distance (km)		Energy demand (kWh)					
	Daily	Annual	Daily			Annual		
			$\eta_{Powertrain}$	$\eta_{Battery}$	$\eta_{Charger}$	$\eta_{Powertrain}$	$\eta_{Battery}$	$\eta_{Charger}$
1	38,2	13943,0	218,89	235,36	253,08	79893,39	85906,87	92372,98
2	76,4	27886,0	437,77	470,72	506,15	159786,78	171813,74	184745,96
3	114,6	41829,0	656,66	706,08	**759,23**	239680,17	257720,61	277118,94
4	152,8	55772,0	875,54	941,45	1012,31	319573,56	343627,48	369491,92
5	191	69715,0	1094,43	1176,81	1265,38	399466,95	429534,35	461864,90
6	229,2	83658,0	1313,32	1412,17	1518,46	479360,34	515441,23	554237,88
7	267,4	97601,0	1532,20	1647,53	1771,54	559253,73	601348,10	646610,86

4.2- Solar resources assessment

4.2.1- Seasonal variation of Solar Radiation and Clearness Index

Local solar resource analysis from PVGIS data indicated an average annual daily GHI of approximately 5.03 kWh/m², and 5.58 kWh/m² at the optimum tilt angle, with peaks of around 6.38 kWh/m^2 in February, and a minimum of around 3.58 kWh/m^2 in June, as summarized in the Table 4.5, and illustrated by the graphic in Figure 4.4. Figure 4.5 illustrates the seasonal typical day curves, showing that effective irradiance occurs primarily between 8:30 AM and 3:30 PM, when irradiance levels exceed 200W/m^2. This period corresponds to the hours of significant solar energy availability for PV generation, and in this study, it also coincides with the daytime layover period, when the buses are not in operation and remain parked for charging. In terms of overall values, the annual global irradiation in Maputo is around and 1.84 MWh/m^2**.** These figures are consistent with previous findings by [79], who reported an annual global irradiation of 1.92 MWh/m^2, reinforcing the reliability of the current estimates.

Table 4.5- Solar resources and climate data

TMY PVGIS-MAPUTO					
Year	**Months**	**GHI (kWh/m²)**	**Kt**	**T 10m(C)**	**W10m (m/s)**
2017	Jan	5,760	0.487	26.8	4.105
2019	Feb	6,388	0.577	25.4	4.373
2020	Mar	5,805	0.598	26.1	4.130
2020	Apr	4,628	0.58	23.0	3.818
2007	May	4,224	0.65	21.6	3.974
2007	Jun	3,582	0.616	19.7	4.225
2007	Jul	4,176	0.679	18.5	3.978
2016	Aug	4,396	0.593	20.8	4.625
2008	Sep	5,158	0.567	22.7	4.515
2014	Oct	4,807	0.452	23.6	5.075
2008	Nov	5,751	0.495	23.2	4.692
2019	Dec	5,735	0.477	26.7	4.425
	Daily Average	**5,034**	**0.564**	**23.175**	**4.328**
	Total Annual	1837,519			

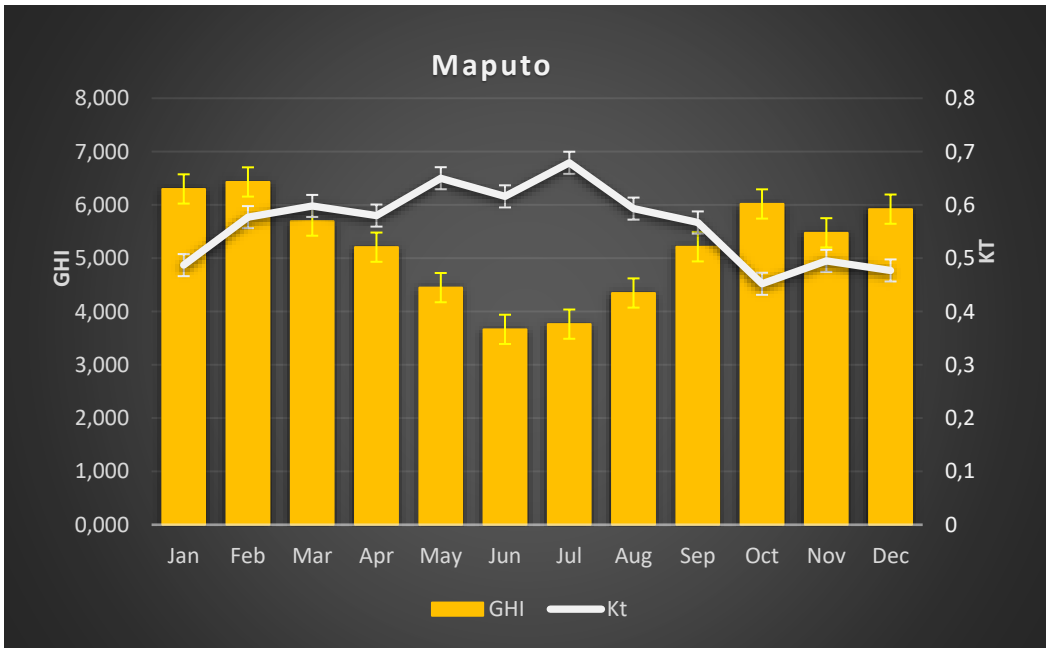


Figure 4.4- Temporal Evolution of the Solar Radiation and Clearness Index in Maputo

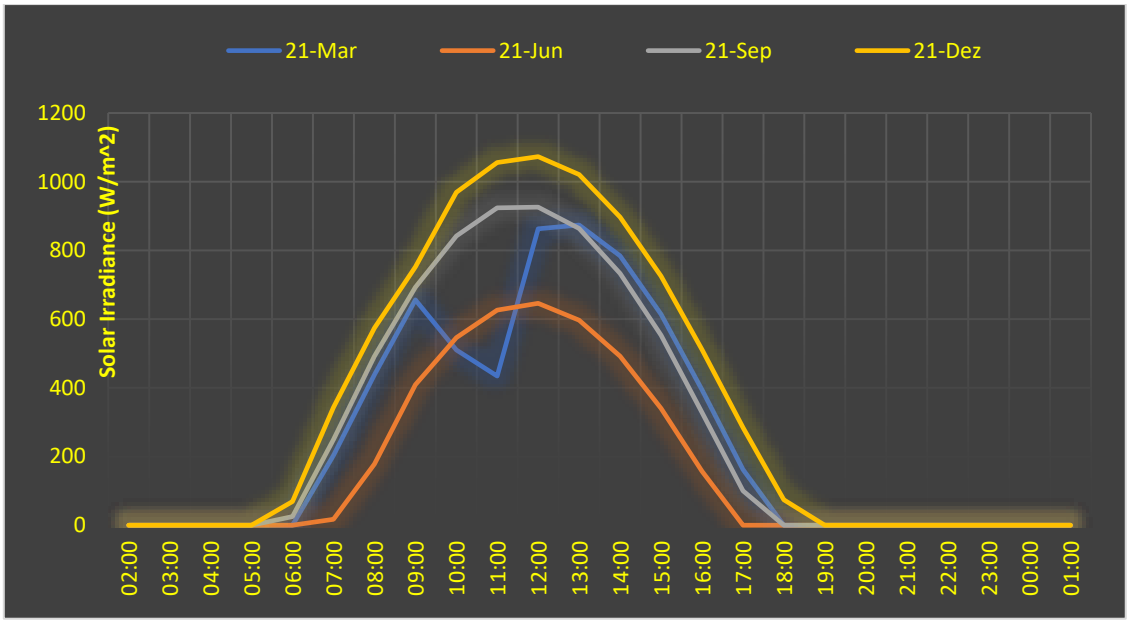


Figure 4.5- Seasonal variability of solar irradiance in Maputo

4.3- PV charging station Design and Sizing

4.3.1- PV System Energy Sizing

The energy sizing of the PV system was carried based on the daily e-buses energy demand. In this context, as presented in Table 4.6, an installed capacity of approximately 220.4 kWp will be required to meet this demand. This corresponds to an estimated array area of 1,345.72 m^2 to 1,725.28 m^2 (depending on the spacing factor of 30% or a GCR of 0.60) and it consists of about 479 modules of the model considered in this study. Note that these are preliminary estimates. A detailed site study should be conducted to account for local conditions, such as shading and terrain, which may affect the actual system performance.

Table 4.6- Load-Driven PV System Dimensioning

	Energy demand (kWh)		PV System Size			
Cycles	**Daily**	**Annual**	**P(kWp)**	**N**	**A(m^2) 30%**	**A(m^2) GCR**
1	253,08	92372,98	73.50	159.675	388,148	497.626
2	506,15	184745,96	146.901	319.349	776,296	995.251
3	**759,23**	**277118,94**	**220.351**	**479.024**	**1,345.72**	**1,492.877**
4	1012,31	369491,92	293.801	638.698	1,552.592	1,990.02
5	1265,38	461864,90	367.251	798.373	1,947.40	2,488.128
6	1518,46	554237,88	440.702	958.047	2,328.888	2,985.753
7	1771,54	646610,86	514.152	1117.722	2,717.035	3,483.379

As outlined in Table 4.2 and Figure 4.3, charging occurs during the midday layover. Taking into account this charging window, a 50 kW CCS Combo 2 charger is considered to meet each

vehicle's energy demand. The energy sizing of the proposed PV system was based on the daily energy demand of the E-Bus fleet. Two sizing scenarios were analysed, both designed to operate under a zero-export constraint. To assess the expected energy yield in each case, throughout the year, simulations were carried out using the PVGIS tool.

4.3.2- PVGIS Simulation for full-demand PV System

i) Scenario 1-Full-demand PV System: In this scenario the PV System is sized to meet 100% of the E-Bus fleet's daily energy demand, even during the least productive month of the year. Surplus energy generated during periods of higher solar production is stored in the BESS. In this context, an installed capacity of approximately 220.4 kWp is simulated. The system achieves an average daily energy output of 920.20 kWh, with seasonal fluctuations ranging from a minimum of 852.5 kWh to a maximum of 991.5 kWh per day.

This configuration results in a consistent daily energy surplus, ranging from 93.2 kWh to 232.2 kWh, with an average of approximately 162.7 kWh per day. Given the system's zero-export constraint, this excess energy is stored in the BESS, which plays a crucial role in absorbing surplus generation and supplying power during periods of low PV output or increased demand. Figure 4.6 presents a visual summary of the projected monthly energy output, while Figure 4.7 illustrates the daily energy balance, highlighting both production levels and surplus energy.

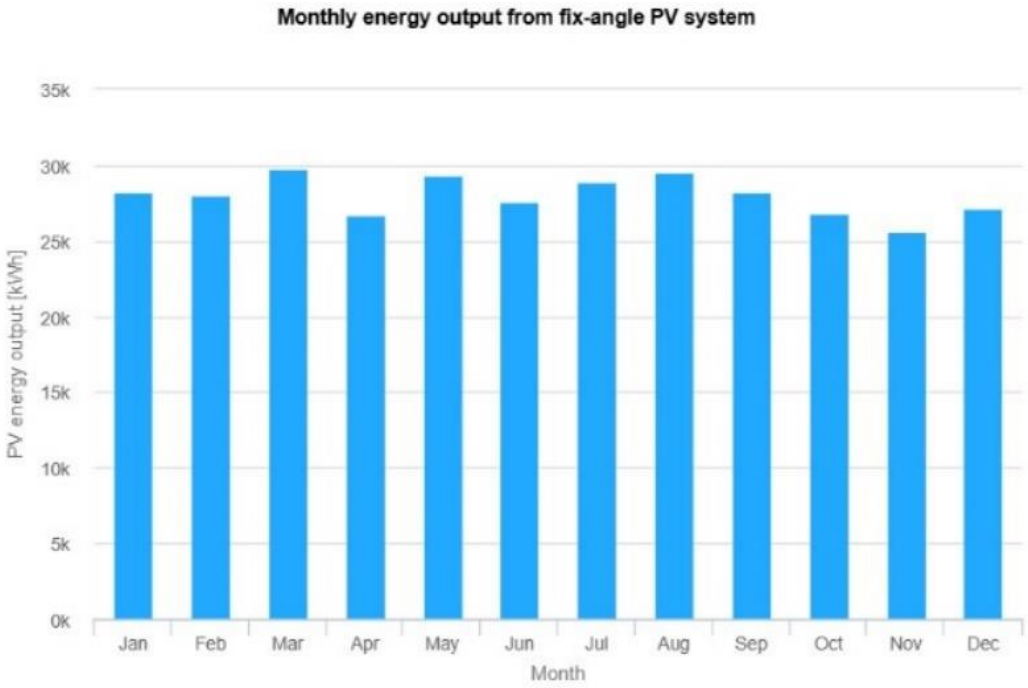
ii) Scenario 2- Demand-Matched PV System Sizing: In this scenario, the PV System is sized to follow the annual average daily energy demand of the e-bus fleet as closely as possible. This design philosophy consists in minimising both surplus and deficit, avoiding unnecessary investment in storage and eliminating excessive surplus that would otherwise require grid injection. With an installed capacity of 181.5 kWp, the system yields an average daily production of approximately 757.78 kWh. Table 4.7 summarises the key input parameters and simulation results obtained from PVGIS tool for both scenarios analysed.

Compared to Scenario 1, the system in this scenario exhibits a narrower seasonal variation, from 702.00 kWh to 816.49 kWh, indicating a more stable generation profile throughout the year. Under this demand-matched sizing approach, the system reaches a maximum surplus of 57.3 kWh and a minimum of -57.2 kWh. The negative value represents a deficit which, in practice, is supplied by the national grid. These two values are almost symmetrical, when averaged over the year, effectively cancels out, yielding a net zero energy balance. This reflects a system that neither consistently overproduces nor undegenerates.

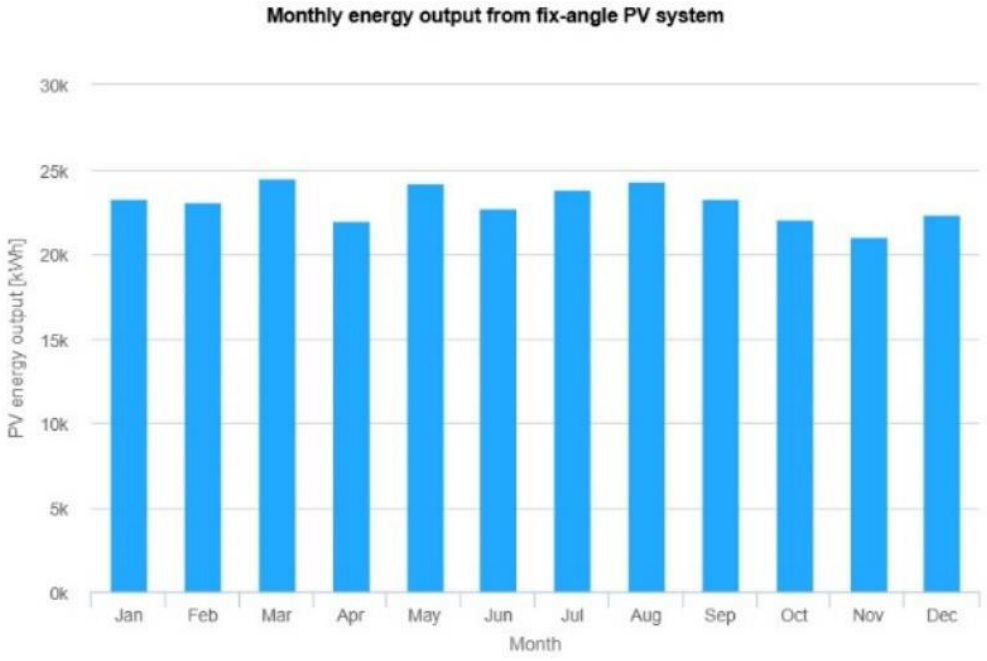
As the system operates under a zero-export constraint and does not include BESS, occasional deficits are covered by the grid, while small surpluses are curtailed. Figure 4.7b illustrates the system's daily energy balance under this scenario, highlighting its balanced and optimised performance.

Table 4.7- PVGIS Input Parameters and Simulated Energy Output

Input parameters:	
Location [Lat/Lon]:	-25.969,32.565
Database used:	PVGIS-SARAH2
PV technology:	Crystalline Silicon (original)
System loss [%]:	14
Slope angle [Â°]:	29 (opt)
Azimuth angle [Â°]:	-179 (opt)
Simulation outputs for Installed Capacity of 220.4 kWp	
Yearly PV energy production [kWh]:	335873.68
Yearly in-plane irradiation [kWh/m2]:	2059.91
Year-to-year variability [kWh]:	7469.60
Simulation outputs for Installed Capacity of 181.5 kWp	
Yearly PV energy production [kWh]:	276592.89
Yearly in-plane irradiation [kWh/m2]:	2059.91
Year-to-year variability [kWh]:	6151.23
Changes in output due to:	
Angle of incidence [%]:	-2.62
Spectral effects [%]:	1.01
Temperature and low irradiance [%]:	-12.55
Total loss [%]:	-26.02

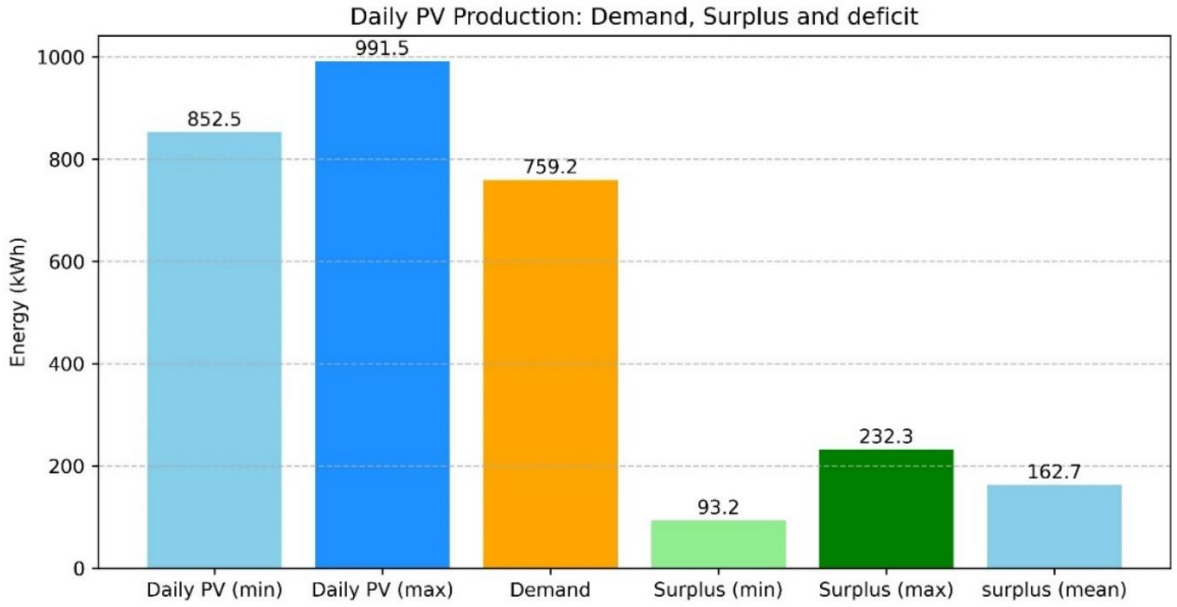


(a)

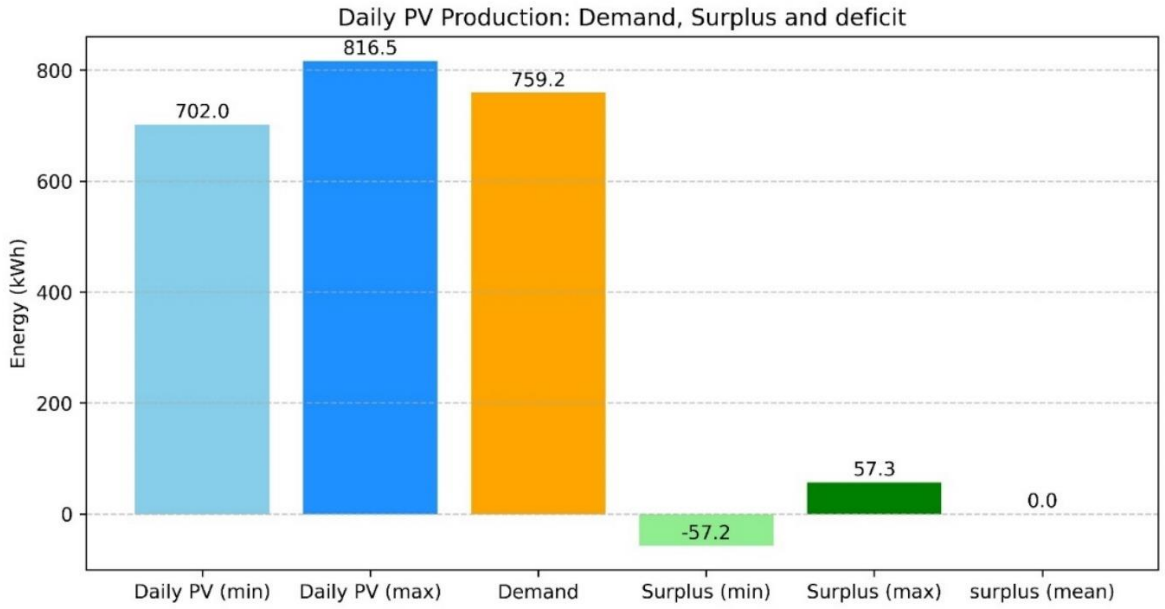


(b)

Figure 4.6- Monthly average PV output (a) 220.4kWp and (b) 181.5 kWp



(a)



(b)

Figure 4.7- Annual profile of daily production extremes and energy balance for the: (a) 220.4kWp and (b) 181.5 kWp systems

4.4- Energy and Environmental Implications

4.4.1- Energy Implications-Comparative Perspective

Three energy supply scenarios were simulated to evaluate the energy and environmental performance of transitioning to electric buses, with or without PV integration. Considering that the fuel consumption of an ICE bus operating in urban-oriented cycles ranges from 0.424L/km

to 0.556L/km [80], [81], and taking into account that the diesel Low Heating Value (LHV) is 10 kWh/L, this fuel consumption interval corresponds to an average energy consumption of approximately 4.90 kWh/km. With these figures, the e-bus shows approximately 58.2% lower consumption than their diesel counterparts for equivalent operational conditions. This difference translates not only into a direct reduction in GHG emissions, but also into significant long-term operational savings, particularly in urban contexts characterised by regular routes and frequent stop-and-go patterns.

The Table 4.7 below summarizes the distance travelled and the correspondent annual fuel/energy consumption per vehicle, based on three round-trips per day. The specific consumption of the EV presented in the Table 4.7 takes into account a battery efficiency of 93%.

Table 4.8- Description of Energy Supply Scenarios

Property	Diesel-Based	Grid charging	PV-based charging
Travelled distance (km/year)	41829.0	41829.0	41829.0
Specific consumption (L/km or kWh/km)	0.49	2.05	2.05
Fuel consumption (L or kWh)	20,496.21	85,906.87	85906,87

4.4.2- Environmental Implications of PV-Based Charging

Based on the annual emissions per vehicle replacing a diesel bus with an E-Bus charged entirely from the grid leads to an approximate 99.98% reduction in CO_2 emissions in-situ. When powered exclusively by PV Charging, CO_2 emissions are eliminated entirely, corresponding to an annual reduction of approximately 164 tCO_2/year. Across all scenarios, both grid and PV, in-situ emissions of NO_x and PM would be completely eliminated. The comparison of annual emissions across these different charging scenarios is shown in Table 4.8. Estimated emissions for each scenario is based on standardized emission factors.

Table 4.9- Comparative Emissions analysis across different scenarios

	Emissions (tons/year)		
Scenario	CO_2	Nox	PM2.5
Diesel-Based	163.97	1.33	0.04
Grid-based	0.036	0.00	0.00
PV-based	0.00	0.00	0.00

Chapter 5 CONCLUSIONS AND RECOMMENDATIONS

5.1- Conclusions

This study evaluated the integration of PV Systems into the charging infrastructure for E-buses operating along the proposed BRT Line N1 in the MMA. The analysis was carried out through an integrated modelling framework that included driving-cycle simulations, solar resource assessments, PV System sizing, and an emission comparison under different energy supply scenarios. Using a physics-based modelling approach, the specific energy consumption of an 18 m articulated E-bus was found to range between 1.30 and 2.52 kWh/km, depending on road gradient, with an average of 1.91 kWh/km at the powertrain level. These results are consistent with values reported for similar urban articulated buses.

Based on the operational schedule of three daily round trips per vehicle, the required PV-supplied daily energy demand for the fleet of three E-buses was estimated at approximately 759 kWh, corresponding to 277 MWh annually. These values define the minimum annual generation required for a PV-based Charging Station supporting the selected fleet. Solar resource analysis using PVGIS tool confirmed favourable conditions for PV deployment, with an annual daily average GHI of 5.03 kWh/m² and a GTI of 5.58 kWh/m² at the optimum tilt angle of 29$^{o.}$ Using this dataset and simulated mobility patterns, two zero-export PV sizing scenarios were assessed.

Scenario 1, sized at 220.4 kWp to meet full daily demand year-round, produced an average surplus of about 162.7 kWh/day. Given the zero-export constraint, this surplus justifies the integration of a BESS. Scenario 2, optimised to match annual average demand, produced a near-zero net surplus, enabling high self-consumption and eliminating the need for a BESS, although occasional deficits are covered by the national grid.

The comparative energy analysis demonstrated that an E-bus system could consume approximately 58.2% less energy per km than diesel buses operating under similar urban conditions. This substantial efficiency advantage translates directly into reduced fuel use and operational costs. Environmentally, replacing a diesel bus emitting approximately 164 tCO_2/year with a grid-charged E-bus could reduce in-situ CO_2 emissions by about 99.98%, while PV-based charging could eliminate them entirely. In both electrification scenarios, in-situ NO_x and $PM_{2.5}$ emissions are fully removed, significantly improving local air quality.

Overall, the findings confirm that integrating PV-based Charging Stations into Maputo's future BRT system is technically viable, environmentally beneficial, and strategically aligned with sustainable mobility objectives. The proposed approach provides a replicable framework for local and other African cities seeking to decarbonize public transport systems through the combined deployment of renewable energy and E-mobility.

5.2- Limitations

Despite the promising outcomes, the study is subject to several limitations such as:

- Data Scarcity and Assumptions: The study relied on simulations and assumptions parameters, which may introduce a degree of uncertainty. For instance, variation in e-bus load profiles could affect system sizing and performance outcomes;
- Operational Variability: Factors such as driver behaviour, route characteristic, operation pattern can significantly affect energy performance, and were not fully captured in this simulation;
- No Economic or WTW Analysis: The study focused on technical and environmental aspects, without addressing a full economic comparison between diesel and PV-based System, or embodied emissions across the complete WTW energy chain;
- Hybrid configurations not explored: Although current BESS cost remains high, future cost reductions and policy incentives could make such configurations more feasible.

5.3- Recommendations for Future Research

To address the study's limitations and expand its scope, further research should consider:

- A Real-world small-scale pilot PV-Based E-bus charging station in the MMA to validate the simulation results;
- A Comprehensive WTW and Economic Feasibility Analyses to capture the complete energy and emission pathways and understand the investment viability;
- A Policy Frameworks and Fiscal Incentive Analysis to understand their role in promoting solar-powered e-mobility and private sector engagement;
- Given that BESS currently represent a major share of the overall cost, an economic viability analysis of Hybrid System Configurations is recommended to assess how projected BESS cost reductions could improve economic feasibility in the near future.

CONFERENCE PAPER PRESENTATIONS

9th E-Mobility Power System Integration Symposium | Berlin, Germany | 06 – 07 October 2025
Submission 282

Solar PV-Based EV Charging Station for Urban Mobility: A Case Study of the proposed BRT Line N1 in the Maputo Metropolitan Area



Manuel Da Costa [1], Luis Chea [2], Boaventura Cuamba [3]

[1] *ISPS, Mozambique*

[2] *UEM, Mozambique*

[3] *UEM, Mozambique*

Motivated by the need to mitigate climate change, reduce urban air pollution, and curb reliance on volatile fuel prices, this study investigates the integration of solar photovoltaic (PV) systems into electric bus (E-bus) charging infrastructure, for the proposed Bus Rapid Transit (BRT) Line N1, in the Maputo Metropolitan Area (MMA). The urban mobility pattern in Maputo is characterized by strong unidirectional flows and peak-hour demand, with inbound trips in the morning and outbound trips in the late afternoon. Accordingly, the operational schedule was defined within peak periods, with three round trips per bus adopted for simulation. The E-bus load profile was defined using a physical model, yielding an average specific energy consumption of 1.91 kWh/km. A solar resource assessment based on PVGIS-SARA2 data indicates an annual daily average global horizontal irradiation (GHI) of 5.2 kWh/m², peaking at 6.4 kWh/m² in February and dropping to 3.7 kWh/m² in June. The PV charging station was sized to meet daily demand and modelled as a grid-connected, zero-export, strict self-consumption system. Results demonstrate both the technical feasibility and scalability of this approach, providing strategies to manage simultaneous peaks in transport and energy demand, thereby contributing to sustainable urban mobility and supporting the energy transition.

@HCB- Revista Técnico-científica, 00:2 (2025) 1-20
ISSN
DOI:

Macroscopic Physics-Based Modeling for Energy Demand Forecasting of Urban E-Buses

Case Study of BRT Line N1 in the Maputo Metropolitan Area

Manuel João Da-Costa
Faculdade de Engenharia, Instituto Superior Politécnico de Songo, Cahora Bassa, Moçambique
(mdacosta200@gmail.com) ORCID 0009-0009-2092-313X

Luis Consolo Chea
Departamento de Física, Faculdade de Ciência, Universidade Eduardo Mondlane, Maputo, Moçambique
(luis.chea09@gmail.com)

ARTIGO INFO

Histórico do Artigo:
Recebido:
Revisto:
Aceite:

Palavras Chaves:
Electric Buses;
EV Energy consumption;
Energy Transition Strategy;
PV Charging Station;
Urban Mobility;
Bus Rapid Transit

Tipo Eixo Temático:
Mudanças climáticas e transição energética

Acesso Aberto
Avaliado Revisores
CC BY

ABSTRACT

This study aims to estimate the specific energy consumption of electric buses (e-buses) in urban contexts, as a function of a set of vehicle, route and operational parameters, with a comparative analysis to diesel buses. Given the significant variability in energy consumption values reported in the literature, ranging from 1.6 to 3.4 kWh/km, and the empirical range from 1.6–1.84 kWh/km, the need for context-specific analysis becomes evident. The vehicle parameters were obtained from the official technical datasheet provided by the manufacturer; route parameters were sourced from OpenStreetMap (OSM); and operational parameters were extracted from the proposed Bus Rapid Transit (BRT) system, as documented in the reports of the Comprehensive Urban Transport Master Plan for Greater Maputo and from OSM data. The results indicate that a round trip per e-bus on the proposed BRT line requires approximately 72.6kWh. This corresponds to an average specific energy consumption of 1.91 kWh/km, within a range of 1.30 to 2.52 kWh/km, depending on road slope, highlighting the sensitivity of energy demand to road gradient. Compared to their diesel-based counterparts (2.4 kWh/km), the e-bus demonstrates an energy advantage of over 20% per km, reinforcing electromobility as not only a cleaner but also more energy-efficient and economically resilient alternative for urban transport systems. However, these figures represent a macroscopic estimate; actual consumption my vary depending on the vehicle, route and operational parameters. This analysis aligns with the fourth pillar of Mozambique's Energy Transition Strategy (ETS) and contributes to the Sustainable Development Goals (SDGs). The outcomes are also critical for designing photovoltaic (PV) charging infrastructure to ensure self-sufficient fleet operation and minimize grid dependency, supporting the future implementation of low-carbon transport systems

SATELLITE DATA-BASED SPATIO-TEMPORAL ASSESSMENT OF SOLAR PV POTENTIAL FOR EV CHARGING INFRASTRUCTURES: A Case Study in the Maputo Metropolitan Area and Vila de Songo

Manuel João Da-Costa
Instituto Superior Politécnico de Songo
E-mail: mdacosta200@gmail.com

Luis Consolo Chea
Universidade Eduardo Mondlane
E-mail: luis.chea09@gmail.com

Boaventura Chongo Cuamba
Universidade Eduardo Mondlane
E-mail: boaventura.cuamba@gmail.com

ABSTRACT
Rapid urban expansion in Mozambique has increased transport demand and energy consumption, making the electrification of public transport and the advancement of electromobility essential. Among the potential solutions, electric buses (E-buses) present a pathway to mitigate emissions and energy security, however, their effectiveness relies on the availability of reliable Electric Vehicles charging infrastructure. Solar photovoltaic energy (SPVE) provides a sustainable solution due to Mozambique's high solar irradiation levels. With a conceptual design based on harnessing SPVE for Electric-Buses (E-Buses) charging, this study presents an assessment of solar PV potential in the Maputo Metropolitan Area (MMA) and Vila de Songo. The aim is to characterize the temporal dynamic of solar irradiation, clearness index patterns, and estimate the specific PV productivity (kWh/kWp). The analysis is based on hourly time series datasets sourced from the PVGIS-SARAH2 and SARAH3 satellite database, using the Typical Meteorological Year (TMY) approach. Crystalline silicon PV technology is considered for energy yield simulations. The results indicate that the annual daily average of Global horizontal irradiation (GHI) is around 5.0 kWh/m^2 in Maputo-Baixa and Zimpeto, while Songo, records higher values, averaging 5.80 kWh/m^2. In Maputo, mid-winter is marked by clear skies and cooler temperatures, with the clearness index (kt) showing regular seasonality. In contrast, for most of the year Songo experiences greater atmospheric variability under partially cloudy conditions ($0.3 \leq kt \leq 0.65$). Simulations with crystalline silicon (c-Si) PV technology indicate that the specific yield in Songo is approximately 12.4% above the MMA average, while Zimpeto exceeds Baixa by about 3.7%. These differences highlight the role of local climatic factors on PV performance. Nevertheless, both regions provide favorable solar potential to support EV charging infrastructure.

KEYWORDS: Solar Photovoltaic Energy, Electric buses, Electric Vehicle Charging, Electromobility

REFERENCES

[1] UNDESA/POP, "World Population Prospects 2022: Summary of Results. UN DESA/POP/2022/TR/NO. 3," 2022. [Online]. Available: www.un.org/development/ desa/pd/.

[2] UNFPA, "State of World Population report 2023," 2023. [Online]. Available: www.unfpa.org/swp2023/YouGovData

[3] H. Ritchie *et al.*, "Population Growth," *Our World Data*, 2023, [Online]. Available: https://ourworldindata.org/population-growth

[4] A. A. da S. Francisco and M. Paulo, "Impacto da Economia Informal na Protecção Social , Pobreza e Exclusão : A Dimensão Oculta da," 2006, [Online]. Available: http://cea.iscte.pt

[5] D. Satterthwaite, "Human Settlements Discussion Paper Series The scale of urban change worldwide 1950-2000 and its underpinnings," 2004.

[6] H. ; Ritchie, V. Samborska, and M. Roser, "Urbanization," *Our World Data*, 2024, [Online]. Available: https://ourworldindata.org/urbanization

[7] SLoCaT, "SLOCAT Transport and Climate Change Global Status Report Tracking Trends in a Time of Change : The Need for Radical Action Towards Sustainable Transport Decarbonisation About the SLOCAT Partnership," 2021.

[8] IEA, "Energy Technology Perspectives 2017 - Tracking Clean Energy Progress," 2017. [Online]. Available: http://www.iea.org/media/etp/Tracking_Clean_Energy_Progress.pdf

[9] IEA, "Energy Balance 2021-2022," Paris, 2023.

[10] INE, "Estatística dos Transportes e Comunicações-2022," *Stat. Port.*, p. 233, 2023.

[11] MIREME, "Estratégia de transição energética 2023-2050," 2023.

[12] B. C. Cuamba, M. L. Chenene, G. Mahumane, D. Z. Quissico, J. Lovseth, and P. O'Keefe, "A solar energy resources assessment in Mozambique," *J. Energy South. Africa*, vol. 17, no. 4, pp. 76–85, 2006, doi: 10.17159/2413-3051/2006/v17i4a3234.

[13] B. M. Hankins, "A Renewable Energy Plan for Mozambique," no. September, 2009.

[14] BRT Standard, "the Brt Standard Introduction Brt Awards Showcase Scoring in Detail Application To," 2016.

[15] Zatran, "Bus Rapid Transit (BRT)." Accessed: Nov. 20, 2024. [Online]. Available: https://www.zatran.com/en/technology/bus-rapid-transit-brt/

[16] JICA, "Comprehensive Urban Transport Master Plan for the Greater Maputo. Pre-Feasibility Study Report," Maputo, 2014.

[17] V. Nelson, *Energy & the Environment: INTRODUCTION TO RENEWABLE ENERGY*. CRC Press. Tylor & Francis Group, 2011. [Online]. Available: http://www.crcpress.com

[18] NASA Space Place, "Life Cycle of the Sun." Accessed: May 08, 2024. [Online]. Available: https://spaceplace.nasa.gov/all-about-the-sun/en/life-cycle-of-the-sun.en.png

[19] H. C. W. Fisk, M. J.; Anderson, *Introduction to Solar Technology*. Addison-Wesley, 1982.

[20] V. Quaschning, *Understanding renewable energy systems*. 2005. doi: 10.4324/9781315800493.

[21] J. A. Duffie and W. A. Beckman, *Solar Engineering of Thermal Processes, Photovoltaics and Wind Emeritus Professor of Mechanical Engineering*, vol. 5. 2020. [Online]. Available: www.wiley.com/go/permissions.

[22] J. A. D. Deceased and W. A. Beckman, *of Thermal Processes Solar Engineering*.

[23] World Bank Group, “Global Solar Atlas – Mozambique: Download Data.”

[24] S.R. Wenham; M.A. Green; M.E. Watt; R. Corkish, *APPLIED PHOTOVOLTAICS.*, 2nd ed. UK, USA, 2007. [Online]. Available: www.earthscan.co.uk

[25] K. A. N. A.-A. Maan J B Buni, Ali A.K. Al-Walie, “Effect of Solar Radiation on Photovoltaic Cell,” *Int. Res. J. Adv. Eng. Sci.*, vol. 3, no. 3, pp. 47–51, 2018.

[26] V. Sun, A. Asanakham, T. Deethayat, and T. Kiatsiriroat, “A new method for evaluating nominal operating cell temperature (NOCT) of unglazed photovoltaic thermal module,” *Energy Reports*, vol. 6, pp. 1029–1042, 2020, doi: 10.1016/j.egyr.2020.04.026.

[27] M. . Fuentes, “A simplified thermal model for Flat-Plate photovoltaic arrays. Report Number: SAND-85-0330 ON: DE87009386,” 1987.

[28] CEPEL-CRESESB, *Manual de Engenharia para SISTEMAS FOTOVOLTAICOS*, Revisada e. Rio de Janeiro, 2014.

[29] H. Max and S. Souza, *Sistemas Híbridos: Soluções Energéticas para a Amazônia*, 1st ed. 2008.

[30] A. Ciocia *et al.*, “Self-Consumption and Self-Sufficiency in Photovoltaic Systems: Effect of Grid Limitation and Storage Installation,” *Energies*, vol. 14, no. 6, pp. 0–24, 2021, doi: 10.3390/en14061591.

[31] G. Merei, J. Moshövel, D. Magnor, and D. U. Sauer, “Optimization of self-consumption and techno-economic analysis of PV-battery systems in commercial applications,” *Appl. Energy*, vol. 168, no. April, pp. 171–178, 2016, doi: 10.1016/j.apenergy.2016.01.083.

[32] E. Garabitos Lara and A. Vallejo Díaz, “Sizing of photovoltaic systems for self-consumption without surpluses through on-site measurements: Case study of the Dominican Republic,” *Renew. Energy*, vol. 236, no. September, p. 121422, 2024, doi: 10.1016/j.renene.2024.121422.

[33] T. Boonraksa, P. Boonraksa, G. Sakulphaisan, and B. Marungsri, “Strategic planning of charging stations for electric public transportation bus systems: A case study,” *Int. Rev. Electr. Eng.*, vol. 15, no. 6, pp. 512–522, 2020, doi: 10.15866/iree.v15i6.18764.

[34] J. W. Restrepo, Andrés Emiro Diez; Kempten , Helmuth Biechl Hochschule; Gonzalez, “STRATEGY TO ELECTRIFY PUBLIC TRANSPORTATION SYSTEMS IN COLOMBIA,” no. November 2010, 2010, doi: 10.13140/2.1.2646.7525.

[35] D. D. Tran, M. Vafaeipour, M. El Baghdadi, R. Barrero, J. Van Mierlo, and O. Hegazy, “Thorough state-of-the-art analysis of electric and hybrid vehicle powertrains: Topologies and integrated energy management strategies,” *Renew. Sustain. Energy Rev.*, vol. 119, no. November, p. 109596, 2019, doi: 10.1016/j.rser.2019.109596.

[36] S. S. G. Acharige and S. Member, “Review of Electric Vehicle Charging Technologies , Standards , Architectures , and Converter Configurations,” *IEEE Access*, p. 39, 2023, doi: 10.1109/ACCESS.2023.3267164.

[37] L. Shams Ashkezari, H. J. Kaleybar, and M. Brenna, “Electric Bus Charging Infrastructures: Technologies, Standards, and Configurations,” *IEEE Access*, vol. 12, pp. 80505–80528, 2024, doi: 10.1109/ACCESS.2024.3410880.

[38] R. Zaino, V. Ahmed, A. M. Alhammadi, and M. Alghoush, “Electric Vehicle Adoption : A Comprehensive Systematic Review of Technological , Environmental , Organizational and Policy Impacts,” 2024.

[39] M. Littwin, F. P. Baumgartner, M. Green, and W. van Sark, *Performance of New Photovoltaic System Designs 2021*. 2021. [Online]. Available: www.iea-pvps.org

[40] IRENE, “Innovation Outlook: Smart Charging For Electric Vehicles,” Abu Dhabi., 2019.

[41] L. Yao, Z. Damiran, and W. H. Lim, “Optimal charging and discharging scheduling for electric vehicles in a parking station with photovoltaic system and energy storage system,” *Energies*, vol. 10, no. 4, 2017, doi: 10.3390/en10040550.

[42] J. Twidell and T. Weir, *Renewable Energy Resources*, 2nd ed. 2006.

[43] S. Rathore, “Dispositivo Controlador de Exportação Zero: Gestão Eficiente de Energia Solar e Controle de Exportação.” Accessed: May 22, 2025. [Online]. Available: https://www.hashstudioz.com/blog/zero-export-controller-device/

[44] Amara NZero, “GRID ZERO.” Accessed: Oct. 20, 2025. [Online]. Available: https://amaranzero.com.br/blog/grid-zero

[45] K. Hoare, “Zero Export Devices For Grid Connect Solar Power Systems,” My Solar Quotes. Accessed: Sep. 18, 2025. [Online]. Available: https://www.mysolarquotes.co.nz/blog/solar-technology/zero-export-devices-for-grid-connect-solar-power-systems/

[46] R. Luthander, J. Widén, D. Nilsson, and J. Palm, “Photovoltaic self-consumption in buildings: A review,” *Appl. Energy*, vol. 142, pp. 80–94, 2015, doi: 10.1016/j.apenergy.2014.12.028.

[47] J. Pastuszak and P. Węgierek, “Photovoltaic Cell Generations and Current Research Directions for Their Development,” *Materials (Basel).*, vol. 15, no. 16, 2022, doi: 10.3390/ma15165542.

[48] M. Di Sabatino, R. Hendawi, and A. S. Garcia, “Silicon Solar Cells: Trends, Manufacturing Challenges, and AI Perspectives,” *Crystals*, vol. 14, no. 2, 2024, doi: 10.3390/cryst14020167.

[49] IRENA and IEA, “End-Of-Life Management: Solar Photovoltaic Panels,” 2016. [Online]. Available: www.irena.org

[50] H. M. Hussein *et al.*, “State-of-the-Art Electric Vehicle Modeling : Architectures , Control , and Regulations,” *Electronics*, vol. 13, no. 3578, 2024, doi: https://doi.org/10.3390/ electronics13173578.

[51] E. Javanmardi, M. Hoque, A. Tauheed, and M. Umar, “Evaluating the Factors Affecting Electric Vehicles Adoption Considering the Sustainable Development Level,” *World Electr. Veh. J.*, vol. 13, no. 120, pp. 0–19, 2023, doi: https://doi.org/10.3390/ wevj14050120.

[52] Fábio Coelho Barbosa, “Battery Electric Bus Technology Review - Current Status and Perspectives.” Accessed: Sep. 24, 2025. [Online]. Available: https://www.sae.org/papers/battery-electric-bus-technology-review-current-status-perspectives-2022-36-0042

[53] W. Barbosa *et al.*, “Electric Vehicles : Bibliometric Analysis of the Current State of the Art and Perspectives,” *Energies*, vol. 15, no. 395, pp. 1–16, 2022, doi: https://doi.org/10.3390/en15020395.

[54] MarketsandMarkets Research, “Electric Bus Market - Global Forecast to 2030,” https://www.marketsandmarkets.com/Market-Reports/electric-bus-market-38730372.html.

[55] Z. Bi, G. A. Keoleian, and T. Ersal, “Wireless charger deployment for an electric bus network: A multi-objective life cycle optimization,” *Appl. Energy*, vol. 225, no. April, pp. 1090–1101, 2018, doi: 10.1016/j.apenergy.2018.05.070.

[56] S. Castellanos, X. Li, and W. Org, “BARRIERS TO ADOPTING ELECTRIC BUSES,” 2019. [Online]. Available: https://www.sustainable-bus.com/wp-content/uploads/2019/05/barriers-to-adopting-electric-buses.pdf

[57] J. A. Manzolli, J. P. Trovão, and C. H. Antunes, “A review of electric bus vehicles research topics – Methods and trends,” *Renew. Sustain. Energy Rev.*, vol. 159, no. February 2021, 2022, doi: 10.1016/j.rser.2022.112211.

[58] IEA, “World Energy Outlook 2025,” 2025, [Online]. Available: www.iea.org

[59] Transdev, “100% sustainably powered e-bus to hit Queensland roads.” [Online]. Available: https://www.transdev.com.au/press-release/100-sustainably-powered-e-bus-to-hit-queensland-roads/

[60] ChargePoint, “ChargePoint Network.” [Online]. Available: https://www.chargepoint.com/

[61] M. Lewis, “This solar + microgrid storage depot can charge 70 electric buses,” electrek. Accessed: Jul. 23, 2025. [Online]. Available: https://electrek.co/2022/10/31/microgrid-solar-charging-station-electric-buses/

[62] Verified Market Reports, “Electric Bus Charging Station Market Size, Competitive Analysis & Forecast 2033,” March 2025. [Online]. Available: https://www.verifiedmarketreports.com/product/electric-bus-charging-station-market/

[63] S. Pelletier, O. Jabali, and G. Laporte, “The electric vehicle routing problem with energy consumption uncertainty,” *Transp. Res. Part B 126 225–255 Contents*, vol. 126, pp. 225–255, 2019, doi: 10.1016/j.trb.2019.06.006.

[64] S. Würtz, K. Bogenberger, U. Göhner, and A. Rupp, “Towards Efficient Battery Electric Bus Operations: A Novel Energy Forecasting Framework,” *World Electr. Veh. J.*, vol. 15, no. 1, 2024, doi: 10.3390/wevj15010027.

[65] A. Jahic, M. Eskander, E. Avdevicius, and D. Schulz, “Energy Consumption of Battery- Electric Buses: Review of Influential Parameters and Modelling Approaches,” *B&H Electr. Eng.*, vol. 17, no. 2, pp. 7–17, 2023, doi: 10.2478/bhee-2023-0007.

[66] C. J. J. Beckers, “Energy Consumption Prediction for Electric City Buses: Using Physics-Based Principles,” Eindhoven University of Tech- nology (TU/e), 2022. doi: 10.6100/94326d40-7f9b-4a77-89fe-4fd4606d9a8f.

[67] M. Gallet, T. Massier, and T. Hamacher, “Estimation of the energy demand of electric buses based on real-world data for large-scale public transport networks Estimation of the energy demand of electric buses based on real-world data for large-scale public transport networks,” no. November 2018, 2018, doi: 10.1016/j.apenergy.2018.08.086.

[68] M. Rogge, S. Wollny, and D. U. Sauer, “Fast charging battery buses for the electrification of urban public transport-A feasibility study focusing on charging infrastructure and energy storage requirements,” *Energies*, vol. 8, no. 5, pp. 4587–4606, 2015, doi: 10.3390/en8054587.

[69] C. De Cauwer, J. Van Mierlo, and T. Coosemans, “Energy consumption prediction for electric vehicles based on real-world data,” *Energies*, vol. 8, no. 8, pp. 8573–8593, 2015, doi: 10.3390/en8088573.

[70] A. Jahic, R. Soliman, M. Eskander, M. Plenz, E. Avdevicius, and D. Schulz, “Investigation of parameters impacting the energy consumption of electric buses,” *IET Conf. Proc.*, vol. 2023, no. 18, pp. 91–98, 2023, doi: 10.1049/icp.2023.2690.

[71] H. S. Levinson, “Bus Rapid Transit on City Streets How Does It Work,” *2nd Urban Str. Symp. (Anaheim, California) — July 28-30, 2003*, pp. 1–25, 2003.

[72] Volvo, “Specifications for Volvo 7900 Electric.” Accessed: Oct. 10, 2024. [Online]. Available: www.volvogroup.com

[73] BRT Standard, “The BRT Standard,” 2016, [Online]. Available: http://www.itdp-china.org/media/publications/pdfs/BRT2016-REV7.pdf

[74] OSMAnd, “OSMAnd Map – Maputo City view.” Accessed: Mar. 25, 2024. [Online]. Available: https://osmand.net/map/plan/#13/-25.9701/32.5391

[75] M. Smets, Arno; Jäger, Klauss; Isabella, Olindo; Swaaij, Rene Van; Zeman, *Solar Energy: The physics and engineering of photovoltaic conversion technologies and systems*. UIT CAMBRIDGE, ENGLAND, 2015.

[76] A. Franco, G. Lutzemberger, M. G. Bevilacqua, F. G. Quilici, and M. Vezzani, "Green-Powered Electric Public Mobility: Integrating Urban and Interurban Routes—A Case Study Analysis," *Electricity*, vol. 5, no. 2, pp. 254–270, 2024, doi: 10.3390/electricity5020013.

[77] P. Sinhuber, W. Rohlfs, and D. U. Sauer, "Study on power and energy demand for sizing the energy storage systems for electrified local public transport buses," *2012 IEEE Veh. Power Propuls. Conf. VPPC 2012*, no. April 2016, pp. 315–320, 2012, doi: 10.1109/VPPC.2012.6422680.

[78] Sustainable-bus, "Electric bus range, focus on electricity consumption. A sum-up," 2023. [Online]. Available: https://www.sustainable-bus.com/news/electric-bus-range-electricity-consumption/

[79] Luis Consolo Chea, Bjorn Karlsson, and Boaventura Cuamba, "Irradiation Analysis for Maputo," *J. Civ. Eng. Archit.*, vol. 6, no. 12, pp. 1654–1662, 2012, doi: 10.17265/1934-7359/2012.12.008.

[80] Franck Landry Bayi Boumal, Ahmed E. Aboud, Sernin Banza Mwanabute, Josepha Fansi Nguietchuan, and Jefferson T. Banquando, "Influence of Driver Behavior on Fuel Efficiency in Intercity Buses: A Simulation-Based Study of the Yaoundé-Douala Corridor in Cameroon," *Acad. J. Sci. Technol.*, vol. 15, no. 3, pp. 27–36, 2025, doi: 10.54097/318gcm24.

[81] L. Grabowski, "Modeling research of city bus fuel consumption for different driving cycles," *J. Phys. Conf. Ser.*, vol. 2130, no. 1, 2021, doi: 10.1088/1742-6596/2130/1/012001.

APPENDIXES

Appendix A- Meteorological Data from PVGIS-SARAH2 (Maputo)

		Irradiance (W/m^2)						T(C)	W(m/s)
Year	month	GHI	GTI_opt	GTI_Lat	GTI-Lat+15	GTI-Lat-15	GTI_Lat+-15	T2m	W10m
2008	Jan	240.009	217.191	221.492	197.487	235.981	235.981	24.804	4.105
2009	Feb	266.185	257.262	260.446	240.119	268.452	268.452	25.469	4.373
2009	Mar	241.867	261.720	262.016	255.121	255.134	255.134	24.366	4.130
2006	Apr	192.835	232.181	229.972	235.292	212.458	235.292	22.872	3.818
2011	May	176.011	242.917	237.823	255.995	206.223	255.995	22.406	3.974
2006	Jun	149.232	214.861	209.583	229.278	178.167	229.278	19.270	4.225
2006	Jul	174.012	251.828	245.659	268.454	208.508	268.454	19.993	3.978
2011	Aug	183.183	234.126	230.699	241.532	207.191	241.532	18.972	4.625
2007	Sep	214.918	243.431	242.569	241.514	230.875	241.514	22.430	4.515
2016	Oct	200.293	199.812	201.586	189.610	226.438	226.438	23.080	5.075
2012	Nov	239.642	221.417	225.417	202.778	237.569	237.569	23.461	4.692
2008	Dec	238.964	212.204	217.016	190.753	233.333	233.333	25.078	4.425
Average		**209.762**	**232.412**	**232.023**	**228.994**	**225.028**	**244.081**	**22.683**	**4.328**

TIME		Irradiance (W/m^2)				
UTC	**UTC+2**	**21-Mar**	**22-Mar**	**21-Jun**	**21-Sep**	**21-Dez**
0:00	2:00	0	0	0	0	0
1:00	3:00	0	0	0	0	0
2:00	4:00	0	0	0	0	0
3:00	5:00	0	0	0	0	0
4:00	6:00	0	0	0	25	69
5:00	7:00	203	205	17	249	343
6:00	8:00	438	438	178	492	574
7:00	9:00	656	653	409	693	752
8:00	10:00	510	811	546	842	969
9:00	11:00	434	923	626	924	1056
10:00	12:00	863	944	646	926	1073
11:00	13:00	874	904	597	864	1021
12:00	14:00	784	792	492	733	897
13:00	15:00	614	615	340	553	725
14:00	16:00	394	391	157	328	511
15:00	17:00	162	158	0	100	284
16:00	18:00	0	0	0	0	74
17:00	19:00	0	0	0	0	0
18:00	20:00	0	0	0	0	0
19:00	21:00	0	0	0	0	0
20:00	22:00	0	0	0	0	0
21:00	23:00	0	0	0	0	0
22:00	0:00	0	0	0	0	0
23:00	1:00	0	0	0	0	0

Appendix B- Daily bus operation at the battery efficiency level

		Distance (km)		EV (kWh)		ICE (kWh)	
Fleet	**Round-Trips**	**Daily**	**Annual**	**Daily**	**Annual**	**Daily**	**Annual**
1	1	38.2	13943.0	78,45	28635,62	187,18	68320,70
	2	76.4	27886.0	156,91	57271,25	374,36	136641,40
	3	**114.6**	**41829.0**	235,36	85906,87	561,54	204962,10
	4	152.8	55772.0	313,82	114542,49	748,72	273282,80
	5	191	69715.0	392,27	143178,12	935,90	341603,50
	6	229.2	83658.0	470,72	171813,74	1123,08	409924,20
	7	267.4	97601.0	549,18	200449,37	1310,26	478244,90

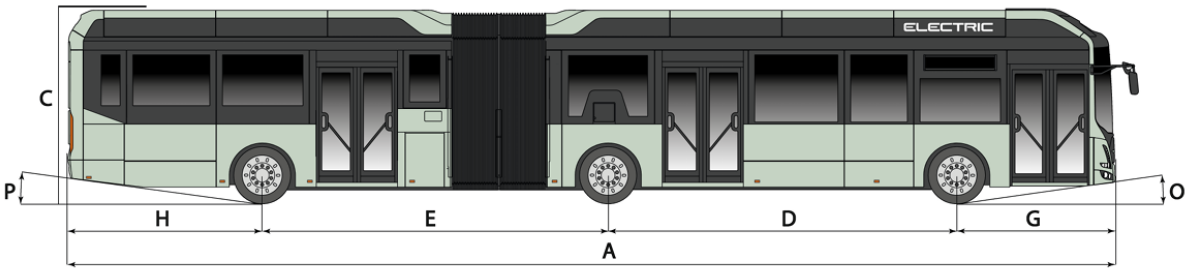
Appendix C- Daily fleet operation at the charger efficiency level

		Distance (km)		EV (kWh)	
Fleet	**Round-Trips**	**Daily**	**Annual**	**Daily**	**Annual**
3	1	38.2	13943.0	253,08	92372,98
	2	76.4	27886.0	506,15	184745,96
	3	**114.6**	**41829.0**	759,23	277118,94
	4	152.8	55772.0	1012,31	369491,92
	5	191	69715.0	1265,38	461864,90
	6	229.2	83658.0	1518,46	554237,88
	7	267.4	97601.0	1771,54	646610,86

ANNEXES

Annex A: Datasheet of VOLVO 7900 articulated E-bus

VOLVO 7900 ELECTRIC ARTICULATED



Model		Articulated, 18.0 m	Articulated, 18.7 m
Overall dimensions			
A	Overall length (mm)	17,849	18,557
	Overall width (mm)	2,550	2,550
C	Overall height (mm)	3,320	3,320
D	Front wheelbase (mm)	5,945	5,945
E	Rear wheelbase (mm)	5,897 (4,037 + 1,860)	6,605 (4,745 + 1,860)
	Max horizontal/vertical turning angle of articulated joint (°)	52/10	52/10
G	Front overhang (mm)	2,699	2,699
H	Rear overhang (mm)	3,308	3,308
O	Approach angle (°)	7.0	7.0
P	Departure angle (°)	7.0	7.0
	Turning radius (outer front corner) (mm)	12,305	12,305
	Turning radius (outer front wheel) (mm)	10,750	10,750
	Overall height, approach and departure angles with tyres	275/70 R22.5	275/70 R22.5

Weights		
Permitted front axle load (kg)	7,500	7,500
Permitted drive axle load (kg)	12,500	12,500
Permitted middle axle load (kg)	10,000	10,000
Permitted GVW (kg)	29,000	29,000

Electrical motor		
Output, max (kW)	R85 max 2x200	R85 max 2x200
	R85 30 min 170	R85 30 min 170
Max wheel torque (Nm)	31,000	31,000

Transmission and axles		
Gearbox	Volvo 2-Speed Automoated, Manual Transmission	Volvo 2-Speed Automated, Manual Transmission
Front axle	Volvo RFS-L	Volvo RFS-L
Rear axle	ZF AV133	ZF AV133
Differential lock	No	No

VOLVO 7900 ELECTRIC ARTICULATED

Charging system
- Two different charging systems available
- Charging time depends on topography, load, climate and drive cycle

Volvo Opportunity Charging (OppCharge)

Maximum charge power 450 kW
Roof-mounted interface, installed above front axle for conductive charging (The same position as on Electric Hybrid)
Fully automatic charging sequence

CCS DC

Maximum charge power 150 kW
Front charging comes as standard
Side and rear charging are optional *
European standard connector
Manual Connection

* Removes front charging. Only one inlet can be installed per vehicle.

Energy storage system
- Lithium-ion battery
- Coolant cooled and heated
- Automatic temperature controlling of batteries

Voltage

600 V

Capacity (total energy)

264- 396 kWh

Cooling system
- Electrically driven fans with improved speed control
- No coolant filter
- Coolant level warning in instrument cluster
- Higher allowed coolant temperature for better cooling performance

Tyres and rims
Steel rims available

Rims	Tyres
7.5 x 22.5"	275/70 R22.5

Air and brake system
- Volvo disc brakes
- Electronic Braking System (EBS 5)
- Anti-lock Braking System (ABS)
- Acceleration Slip Regulation (ASR)
- Brake blending
- Hill Start Aid
- Brake temperature warning
- Poor brake performance warning
- Door brake
- Brake Assistant
- Lining wear sensing and analysis
- Automatic calibration after brake pad change
- Compressed air system, easily filled from external circuit

Exterior and structure
- Volvo's patented lightweight aluminium body concept
- Front and rear wall in composite material and ABS elements
- Front and rear structure in anti-corrosion steel
- Double tinted glazing
- Multilayer exterior paint finish
- Easy repair of minor damages
- Parts commonality between city and intercity buses to lower maintenance cost
- Anti-corrosion treatment of underbody with conservation sealing and silencing agents
- LED headlamps
- LED Daytime running lights
- Auxiliary lights and fog lights as options
- Electrically adjustable and heated external mirrors

Doors and door system
- Electric door system
- Inward gliding and outward sliding doors available
- Double glazing in all doors
- Electric sensitive edge for increased passenger safety

VOLVO 7900 ELECTRIC ARTICULATED

Climate system

- Roof-mounted HVAC unit (Heating, Ventilation and Air Conditioning, including heat pump functionality)
- Pipe convectors and air blowers
- Air blowers at doors
- Defroster with AC
- Driver convector or blower
- Auxiliary diesel/electric heater
- Separate climate zones for driver and passengers
  - For optimal climate and energy efficiency, the passenger temperature is controlled by a pre-set temperature curve
- The temperature in the driver's area is manually controlled

AC unit:
Cooling capacity max (35/40/47%)
31 kW
Heating capacity at Q80
56 kW

Roof heating unit (when not specified with AC):
Heating capacity at Q80
50 kW
9 kW Heat pump (Air/Air)

Convectors:
Heating capacity at Q100
918 W/m

Defroster:
Heating capacity at Q80
18 kW
Cooling capacity max
5.5 kW
Airflow max at dP 0
880 m³/h

Driver AC:
Electrical roof-mounted driver AC, connected to defroster

Auxiliary heater:
Heating capacity
41 kW (18 kW electric and 23 kW fuel)

Interior

- Spacious and bright
- Comfortable
- Integrated position for passenger
- Information displays
- Interior LED lights

Passenger seats

Volvo city seats featuring:

- Optimised city bus seat
- Easy maintenance
- Available in a wide range of specifications to meet the demands of individual customers

Driver's seat and station

- Volvo dashboard
- Dashboard moves with the steering column in height and tilt
- Instrument cluster:
- - speedometer
  - power meter
  - 4.3" display
  - indicators
  - warning lamps
- Volvo Alcolock
- Outdoor temperature meter
- ISRI driver's seat

Electrical system

Automatic shut off of main switch at low voltage level

Number of batteries
2 x 12 V

Battery capacity
105 Ah

Audio system

- Stereo radio with DAB
- Foot controlled public address system
- Amplifier adapted to city bus

Ready to run

- The bus will keep the batteries in working temperature, to ensure that the bus can be started directly when needed without pre-heating period
- 24V batteries will be charged from 600V battery
- Pre-heating of interior can be done via setting timer

Annex B: Characteristic of the Charger considered in this study

Charging Station

DC EV Charger 25 kW - 50 kW, 30 kW - 60 kW

- Self-developed controller for CHAdeMO and CCS
- Supports multiple charging standards: GB, CCS1, CCS2 and CHAdeMO
- Compact size with fashion LED design
- Supports up to 2 Evs
- Built-in RFID card reader
- Supports OCPP 1.6 JSON network and 3G/4G
- Remote firmware upgrade with APP (OTA)
- Remote power module upgrade (OTA)
- Remote diagnostic function simplifies data collection and analysis process
- IP54 protection, IK10 vandal-proof enclosure and IK8 touch screen
- 7" colored touch LCD display for easy configuration



Applications

- Movie theaters, museums,hotels, restaurants, department stores, malls
- Convenient stores, coffeeshops, supermarkets, fast food restaurants, banks
- Parking space, roadside charging

Hightlights



Charging Station

Specification

MODEL		25kW	50kW	30kW	60kW
Charging Type		DC fast charging			
Outlet Options		C: CCS2 cable , A: CCS1 cable , J: CHAdeMO cable , G: GBT cable			
AC Input Power @ 400V 50Hz		40 A, 28 kVA	78 A, 54 kVA	40 A, 28 kVA	93 A, 64 kVA
Input Voltage Range		400 VAC or 380 VAC +/- 10%			
Input Frequency		50 Hz or 60 Hz			
DC Output Power Rating		25 kW	50 kW	30 kW	60 kW
DC Output Voltage		200-750 Vdc (ready) 200-1000 Vdc (coming soon)			
Number of EV Served		Up to 2 (JC, JA models) Up to 1 (C, A, J, G models)	Up to 2 (CC, AA, JC, JJ , GG models) Up to 1 (C, A, G models)	Up to 2 (JC, JA models) Up to 1 (C, A, J, G models	Up to 2 (CC, AA, JC, JJ , GG models) Up to 1 (C, A, G models)
Cable Length		5.0 m, Optional: 6.0 m / 7.0 m			
Maximum Current	CCS Cables	80A	150A	80A	150 A
	CHAdeMO Cables	60A	125A	60A	125 A
	GBT Cables	60A	150A	60A	150 A
Electro-Magnetic Compatibility		Class A (optional Class B) according to EN 61000-6-3:2007			
Distribution Systems		TN-S. TN-C, TN-C-S, TT (required external RCD)			
Connector Type		3P + N + PE			
Protection		Overcurrent, overvoltage, undervoltage, integrated surge protection, ground fault including DC leakage protection, door opening protection			
Overvoltage Category		Type II			
Power Factor (Full Load)		≥ 0.98	≥ 0.99	≥ 0.98	≥ 0.99
THDi		≤ 5%			
Efficiency		≥ 93% (peak)			
Standby Power		< 35 W			
Short Circuit Current		10 kA			
Pre-charge Current		< 1 A			
Inrush Current		< 55 A	< 90 A	< 55 A	< 100 A
Leakage Current		0.8 mA			
Energy Metering		Standard: Meter for DC outlet, Optional: AC inlet			
Cellular Communication		GSM / 4G/ LTE (Optional)			

USER INTERFACE				
Connectivity	Internet access via 4G/3G/Ethernet (RJ45)			
User Authentication	RFID, QR code			
User Interface	7" LCD high-contrast touchscreen			
Communiation Protocols	Proprietary and OCPP 1.6J			
RFID Reader	ISO/IEC 14443 A/B Mifare RFID reader			
Emergency Button	Yes			
Language System	English, Chinese			
GENERAL CHARACTERISTICS				
Protection Rating	IP54 and IK10 (cabinet) / IK8 (touchscreen)			
Housing Material	SGCC, SUS430(Optional)			
Operating Altitude	Up to 2000 m			
Operating Temperature	-35 °C to 55 °C			
Storage Temperature	-40 °C to 70 °C			
Humidity	20-95 % Rh non-condensing			
Mounting	Free-standing cabinet			
Dimensions (D x W x H) mm	660 × 218 × 1250 mm			
Weight (kgs)	80	100	80	100
COMPLIANCE STANDARDS				
Charging System	IEC 61851-1 ed 3, IEC 61851-21-2 ed 1, IEC 61851-23 ed 1, IEC 61851-24 ed 1, IEC 62196-2, IEC 62196-3, IEC 61000,GBT18487, GBT20234			
Communication to the EV	DIN 70121, ISO/IEC 15118 ed 1, CHAdeMO 1.2, GBT27930, GBT 34657			

Product specifications are subject to change without further notice

www.voltronicpower.com

Annex C: Physics model input parameters

Parameter	Value	Source
v [m/s]	9.722	[16]
M [kg]	29000	[72]
g[m/s2]	9.81	
$\theta[rad]$	to calculate	
Cr	0.015	[77]
Cd	0.7	[67]
Af[m2]	7.466	[72]
$\rho[kg/m3]$	1.25	
a[m/s2]	0.981	
η	0.75	
η_m	91	[67]
η_{TG}	95	[77]
η_i	95	[67], [77]
η_{reg}	0.6	[67]

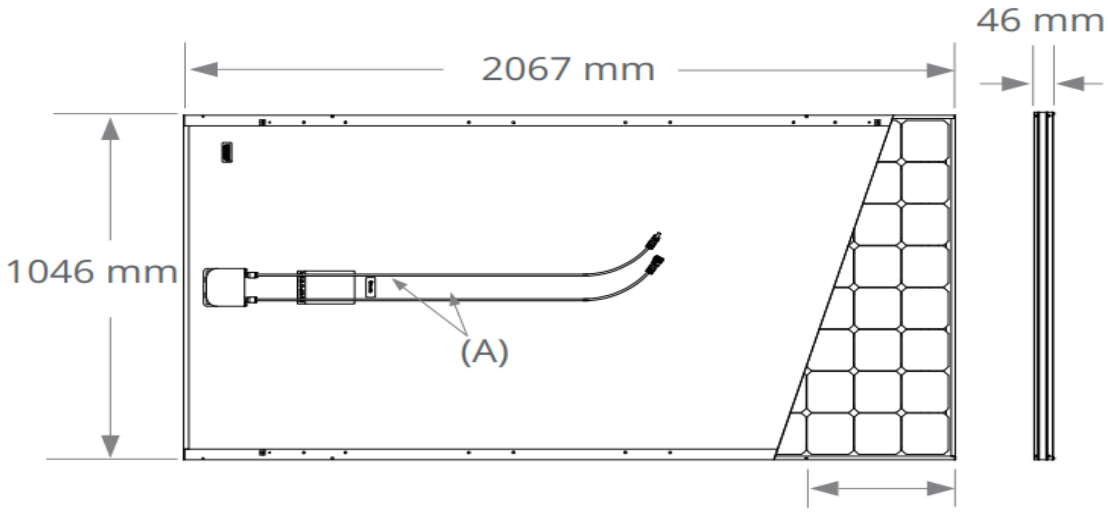
Annex D: Characteristic of the PV modules considered in this study

X-Series: X21-460-COM DC SunPower® Commercial Panel

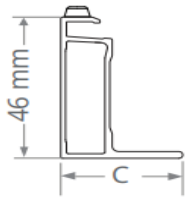
Electrical Data	
	SPR-X21-460-COM
Nominal Power (Pnom) [7]	460 W
Power Tolerance	+5/0%
Panel Efficiency	21.3%
Rated Voltage (Vmpp)	77.3 V
Rated Current (Impp)	5.95 A
Open-Circuit Voltage (Voc)	90.5 V
Short-Circuit Current (Isc)	6.39 A
Max. System Voltage	1500 V IEC & 1500 V UL
Maximum Series Fuse	15 A
Power Temp Coef.	−0.29% / ° C
Voltage Temp Coef.	−223.2 mV / ° C
Current Temp Coef.	2.9 mA / ° C

Operating Condition And Mechanical Data	
Temperature	−40° C to +85° C
Impact Resistance	25 mm diameter hail at 23 m/s
Appearance	Class A
Solar Cells	128 Monocrystalline Maxeon Gen III
Tempered Glass	High-transmission tempered anti-reflective
Junction Box	IP-65, 1230 mm cables / PV4S
Weight	25,4 kg
Max. Load	Wind: 2400 Pa, 244 kg/m² front & back Snow: 5400 Pa, 550 kg/m² front
Frame	Class 2 silver anodized; stacking pins

Tests And Certifications	
Standard Tests [8]	IEC 61215, IEC 61730, UL1703 (Type 2 Fire Rating)
Quality Management Certs	ISO 9001:2015, ISO 14001:2015
EHS Compliance	RoHS, OHSAS 18001:2007, lead free, Recycle Scheme, REACH SVHC-163
Sustainability	Cradle to Cradle Certified™ Silver. "Declare." listed.
Ammonia Test	IEC 62716
Desert Test	10.1109/PVSC.2013.6744437
Salt Spray Test	IEC 61701 (maximum severity)
PID Test	1500 V: IEC 62804, PVEL 600 hr duration
Available Listings	TUV, UL, MCS, FSEC, CEC



FRAME PROFILE



(A) Cable Length: 1230 mm +/-10 mm
(B) Stacking Pins
(C) Long Side: 32 mm
Short Side: 22 mm